



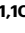






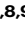


Schwann cell C5aR1 co-opts inflammasome NLRP1 to sustain pain in a mouse model of endometriosis

Received: 8 March 2024

Accepted: 8 November 2024

Published online: 25 November 2024

 Check for updates

Mustafa Titiz ^{1,10}, Lorenzo Landini ^{1,10}, Daniel Souza Monteiro de Araujo ^{1,10}, Matilde Marini ¹, Viola Seravalli², Martina Chieca ¹, Pasquale Pensieri¹, Marco Montini³, Gaetano De Siena¹, Benedetta Pasquini⁴, Silvia Vannuccini⁵, Luigi Francesco Iannone¹, Thiago M. Cunha ⁶, Giulia Brancolini ⁷, Elisa Bellantoni¹, Irene Scuffi¹, Alessandra Masticci ¹, Martina Tesi ¹, Mariarosaria Di Tommaso², Felice Petraglia⁵, Pierangelo Geppetti ^{1,8,9}, Romina Nassini ¹ ✉ & Francesco De Logu ¹ ✉

Over 60% of women with endometriosis experience abdominopelvic pain and broader pain manifestations, including chronic back pain, fibromyalgia, chronic fatigue, vulvodynia, and migraine. Although the imbalance of proinflammatory mediators, including the complement component C5a, is associated with endometriosis-related pain, the mechanisms causing widespread pain and the C5a role remain unclear. Female mice and women with endometriosis exhibit increased plasma C5a levels and pain. We hypothesize the Schwann cells involvement in endometriotic pain. Here, we show that silencing the C5a receptor (C5aR1) in Schwann cells blocks the C5a-induced activation of the NLRP1 inflammasome and subsequent release of interleukin-1 β (IL-1 β). Macrophages, recruited to sciatic/trigeminal nerves by IL-1 β from Schwann cells, increase oxidative stress, which activates the proalgesic TRPA1 pathway, resulting in widespread pain. These findings reveal a pathway involving Schwann cell C5aR1, NLRP1/IL-1 β activation, macrophage recruitment, oxidative stress, and TRPA1 engagement, contributing to pain in a mouse model of endometriosis.

Endometriosis, caused by superficial peritoneal/deep infiltrating implants or ovarian cysts of endometrial-like tissue¹, is an enigmatic and often debilitating gynecologic condition that affects 10–15% of reproductive-aged women². The socioeconomic burden of the disease

is high, as endometriosis affects career, everyday activities, sexual and nonsexual relationships, and quality of life³. More than 60% of women diagnosed with endometriosis suffer from abdominopelvic pain⁴, and often suffer from pain conditions in anatomical sites other than the

¹Department of Health Science, Clinical Pharmacology and Oncology Section, University of Florence, Florence, Italy. ²Department of Health Science, Obstetrics and Gynecology Section, University of Florence, Florence, Italy. ³Department of Experimental and Clinical Biomedical Sciences “Mario Serio”, Medical Genetics Unit, University of Florence, Florence, Italy. ⁴Department of Chemistry “U.Schiff”, University of Florence, Florence, Italy. ⁵Department of Experimental and Clinical Biomedical Sciences, Obstetrics and Gynecology Unit, University of Florence, Florence, Italy. ⁶Center for Research in Inflammatory Diseases (CRID), Department of Pharmacology, Ribeirão Preto Medical School, University of São Paulo, São Paulo, Brazil. ⁷FloNext srl, Florence 50123, Italy. ⁸Department of Molecular Pathobiology, College of Dentistry, New York University, New York, NY 10010, USA. ⁹Pain Research Center, College of Dentistry, New York University, New York, NY 10010, USA. ¹⁰These authors contributed equally: Mustafa Titiz, Lorenzo Landini, Daniel Souza Monteiro de Araujo.

✉ e-mail: romina.nassini@unifi.it; francesco.delogu@unifi.it

pelvis/abdomen, such as chronic back pain, fibromyalgia, vulvodynia, and migraine^{5,6}. Migraine, the most debilitating condition for women aged 20–50 years, is frequent in women with endometriosis in reproductive age^{7,8}. A correlation between fibromyalgia and endometriosis has been proposed, given that immune mechanisms appear to contribute to chronic pain in the two conditions^{9,10}.

The complement system is a broad network of soluble and cell-surface proteins distributed throughout body fluids and tissues with no, or little, basal activity^{11,12}. The complement system acts not just as a first line of defense against pathogens, as it functionally connects innate and adaptive immune responses via receptors expressed by myeloid and non-myeloid cells^{13,14}. Activation of the complement system cascade involves a C3-convertase that cleaves C3, producing C3a and C3b. Two C3b molecules plus the Bb factor form the C5 convertase that cleaves C5 in C5a and C5b^{13,14}. C5a targets a G protein-coupled receptor (GPCR), C5a receptor type 1 (C5aR1), originally identified in neutrophils and monocytes/macrophages¹⁵. C5a contribution in post-operative^{16,17}, inflammatory¹⁸, and neuropathic¹⁹ pain has been previously proposed.

Endometriosis patients undergoing surgery are classified in four stages according to the Revised Classification of Endometriosis by the American Society of Reproductive Medicine (r-ASRM²⁰). Women at the early (I–II) stages have shown higher C5a serum levels compared to controls²¹. Macrophages play a pivotal role in neurogenesis processes occurring close to endometriotic lesions, suggesting their role in endometriosis-associated pain generation^{22–24}. Activation of C5aR1 in endoneurial macrophages induces the NLRP3 inflammasome-dependent release of the pro-nociceptive mediator interleukin 1 (IL-1) β to maintain pain in a mouse model of peripheral nerve injury²⁵. Recently, we showed that crosstalk between Schwann cells (SCs) and endoneurial resident monocytes/macrophages in peripheral nerves activates an oxidative stress pathway that elicits neuroinflammation and sustains chronic pain^{26–29}.

Here, we investigated the mechanism underlying mechanical allodynia produced by endometriotic lesions in the abdomen and other areas distant from the abdomen of female mice, such as the periorbital area to mimic migraine pain and the hind paw to mimic a more widespread pain like that associated with fibromyalgia. As we observed that abdominal mechanical allodynia produced by endometriotic lesions was associated with mechanical allodynia in the hind paw and periorbital area, we explored the cellular and molecular pathway implicated in the mechanical hypersensitivity at the two sites distant from endometriotic lesions. We found that C5a increased by endometriosis, targeting the SC C5aR1, activates the NLRP1 inflammasome, which induces the release of IL-1 β . Increase IL-1 β levels in peripheral nerves (periorbital and sciatic nerves) promote macrophage recruitment. The subsequent release of reactive oxygen species (ROS) targets non-neuronal cells to sustain the oxidative burst and, finally, neuronal transient receptor potential ankyrin 1 (TRPA1) to signal pain. These results implicate SC C5aR1 as a target for the treatment of endometriosis-associated pain.

Results

The complement component C5a mediates endometriosis-induced allodynia

In C57BL/6J female (B6) mice, intraperitoneal (i.p.) injection of dissected uterus horns from donor female mice induced a time-dependent increase in endometriosis-like lesions (Supplementary Fig. 1a), which were associated with prolonged (28 days) periorbital mechanical allodynia (PMA), hind paw mechanical allodynia (HMA), abdominal mechanical allodynia (AMA) and non-evoked pain behavior (i.e., abdominal licking) (Fig. 1a, and Supplementary Fig. 1b). The simultaneous development of allodynia in anatomical areas distant from the abdomen supports the hypothesis that diffusible cellular or molecular mediators are implicated in the widespread proalgesic

response. Several inflammatory cytokines/chemokines have been implicated in endometriotic pain³⁰. The relative levels of forty cytokines/chemokines and acute phase proteins in plasma samples of endometriotic and sham B6 mice were investigated by a proteome profiler array at day 7 after surgery (Fig. 1b). The array revealed increased C5a levels in endometriotic mice (Fig. 1b), and the increase was confirmed by a C5a single analyte ELISA assay both in plasma and tissue lesion samples (Fig. 1c, and Supplementary Fig. 1c). A recent report showed that serum levels of C5a were higher in early stage (I–II) endometriotic than in control patients²¹. Here, we confirmed the higher serum levels of C5a in a group of women with endometriosis ($n=19$) compared to healthy women without endometriosis ($n=15$) (Fig. 1d). In addition, we observed that, in endometriotic B6 mice, C5a plasma levels increased from day 1 to day 8 to then decline to basal levels at day 12–16 after surgery (Fig. 1e).

As C5a has been implicated in several pain conditions^{16–19}, we tested whether the selective allosteric C5aR1 inhibitor, DF2593A, given according to two different temporal schedules would have reduced PMA, HMA, and AMA in endometriotic mice. Endometriotic B6 mice treated with DF2593A (intragastric, i.g., twice a day) from one day before until day 6 after the injection of the ectopic tissue, when C5a levels increase in mouse plasma, showed significantly reduced PMA, HMA, and AMA (Fig. 1f). Conversely, daily treatment with DF2593A, from day 12 to day 16, failed to reduce PMA, HMA, and AMA (Fig. 1g). DF2593A treatment (i.g. twice a day for 6 consecutive days) did not affect either body weight or motor coordination in control B6 mice (Supplementary Fig. 1d). C5b, which is also generated from C5, can combine with the C6 complement component to form the membrane attack complex (MAC)³¹. To exclude the role of the C5b fragment in the present model of widespread pain, endometriotic B6 mice were treated with a C6 antisense oligonucleotide (ASO) (from one day before until day 6 after the injection of the ectopic tissue) that, by inhibiting C6, blocks MAC formation³². Although the C6 ASO treatment reduced C6 expression in liver tissue homogenates from endometriotic B6 mice, (Supplementary Fig. 1e) it failed to reduce PMA, HMA, and AMA (Supplementary Fig. 1f). Overall, the data indicate that, although transient (from day 2 to day 10 after surgery), the increase in C5a plasma levels was sufficient to initiate and sustain PMA, HMA, and AMA.

Neuronal macrophages mediate endometriosis-induced mechanical allodynia

Immune cells, including macrophages and nerve fibers, interact to promote pain symptoms associated with endometriosis^{33,34}. Our previous findings proposed that macrophages infiltrating peripheral nerve trunks interact with SCs to sustain mechanical allodynia in different mouse models of pain^{26–29}. To understand whether macrophage are implicated in the present endometriosis model of widespread pain, their levels were examined in sciatic and trigeminal nerve trunks. Due to the limited size of mesenteric nerve trunks close to endometriotic lesions these were not studied. The number of F4/80⁺ macrophages inside sciatic and trigeminal nerve trunks increased in a time-dependent manner starting from day 3 after surgery (Fig. 2a). The F4/80⁺ cells increase was associated with augmented C5a levels in sciatic and trigeminal nerve homogenates (Fig. 2b).

To explore the role of macrophages in endometriosis-induced mechanical allodynia, macrophage Fas-induced apoptosis (MaFIA) mice, injected with the apoptosis inducer, AP20187, which abates the number of macrophages (GFP⁺/F4/80⁺ cells)³⁵, were used. Ectopic tissue inoculation in the peritoneum of MaFIA mice induced time-dependent PMA, HMA, and AMA, as observed in B6 mice (Fig. 2c). To better understand the action of C5a on SCs and macrophages, MaFIA mice were injected with AP20187 to deplete macrophages following three different time schedules: i) before the increase in C5a levels (from day –2 to day 2); ii) during the C5a increase (from day 2 to day 6);

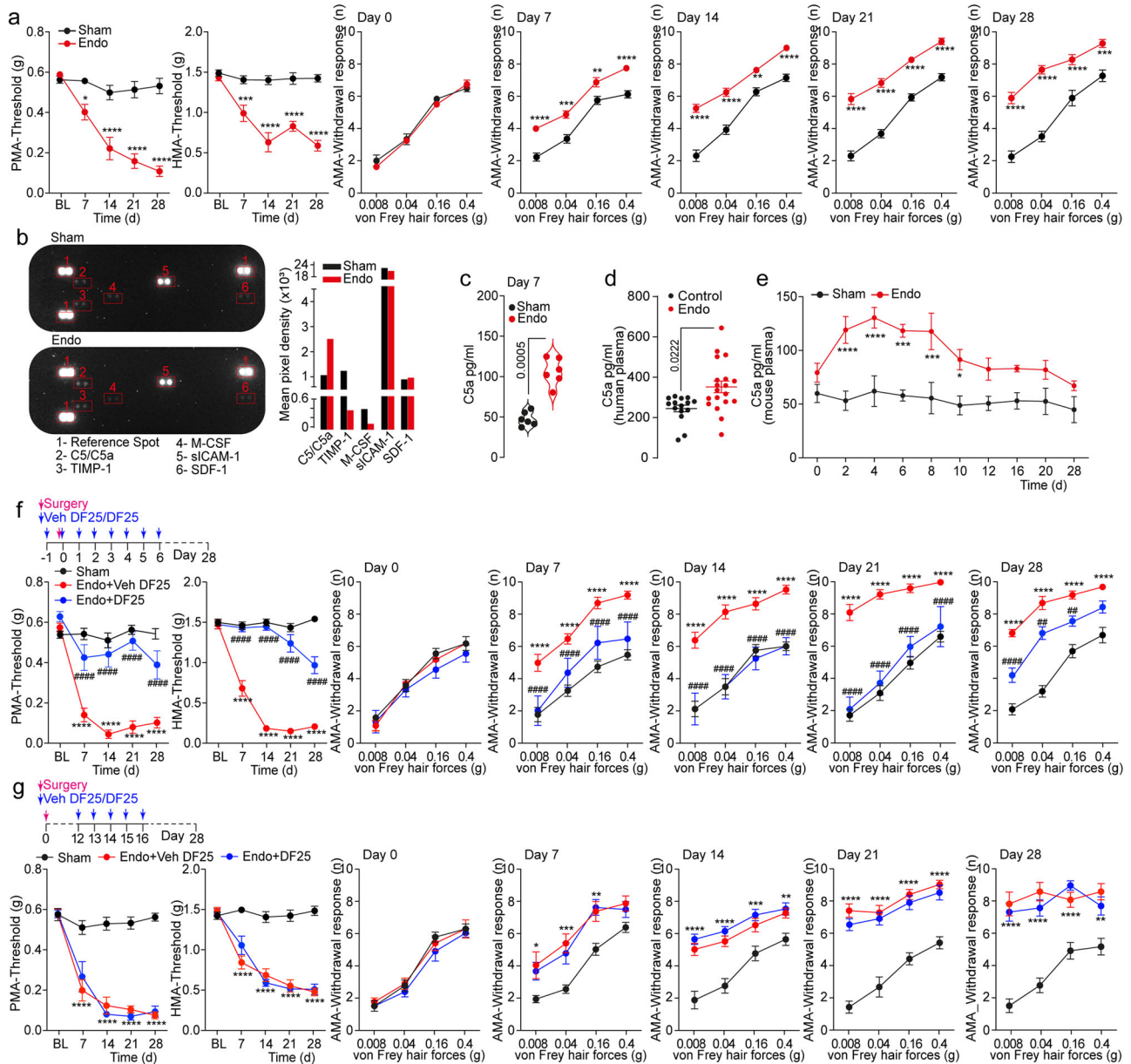


Fig. 1 | Endometriosis-associated mechanical allodynia is mediated by the complement system C5a. **a** Time-dependent periorbital (PMA), hind paw (HMA) and abdominal (AMA) mechanical allodynia in endometriotic (endo) or Sham C57BL/6J female (B6) mice. Proteome profiler array (**b**) and single analyte C5a assay (**c**) in plasma samples from endo and Sham B6 mice. **d** C5a assay in plasma samples from endo patients ($n = 19$) or healthy subjects ($n = 15$) (control). **e** Time-dependent C5a levels in plasma samples from endo and Sham B6 mice. **f** and **g** Timeline of the

DF2593A (DF25) treatment schedule and time-dependent PMA, HMA, and AMA in endo B6 mice after intragastric (i.g.) administration of DF25 (1 mg/kg) or vehicle (Veh) and Sham mice. ($n = 8$ mice per group). Data are mean \pm s.e.m. **a, e, f, g** 2-way ANOVA, Bonferroni correction; **c, d** 2-tailed Student's *t* test. * $P < 0.05$, ** $P < 0.01$, *** $P < 0.001$, **** $P < 0.0001$ vs. Sham ## $P < 0.01$, #### $P < 0.0001$ vs. Endo+Veh DF25. Source data are provided as a Source Data file.

and iii) when C5a declined to baseline (from day 21 to day 25). Macrophage depletion obtained with the two later (ii and iii) (Fig. 2c,d and Supplementary Fig. 1g, h respectively), but not with the early (i) (Supplementary Fig. 1i,j) treatment schedules reduced PMA, HMA, and AMA. These findings are consistent with the transient (~48 hours) monocyte/macrophage depletion obtained in MAFIA mice³⁶. Depletion of monocytes/macrophages in MAFIA mice after AP20187 treatment was evaluated as the number of F4/80⁺ cells in both sciatic and trigeminal nerves (Fig. 2d, Supplementary Fig. 1h, j).

The C5aR1 inhibitor, DF2593A, given to endometriotic mice during the time period when plasma C5a was increased (from day 2 to day 6), reduced macrophages in sciatic and trigeminal nerve tissues (Supplementary Fig. 2a). In contrast, DF2593A treatment when C5a

serum levels declined (from day 12 to 16) failed to affect macrophage accumulation (Supplementary Fig. 2b). Collectively, our data suggest that C5a release, most likely from ectopic endometrial lesions during the first seven days after surgery, increases macrophages in nerve trunks. However, when C5a serum levels decline, the increased number of neural macrophages promotes PMA, HMA, and AMA in a C5a-independent manner.

Schwann cell C5aR1 mediates macrophage recruitment and endometriosis-induced mechanical allodynia

Given that in several mouse models of pain, SCs play a crucial role in sustaining mechanical allodynia, we investigated whether these glial cells contributed to PMA, HMA, and AMA in the present model of

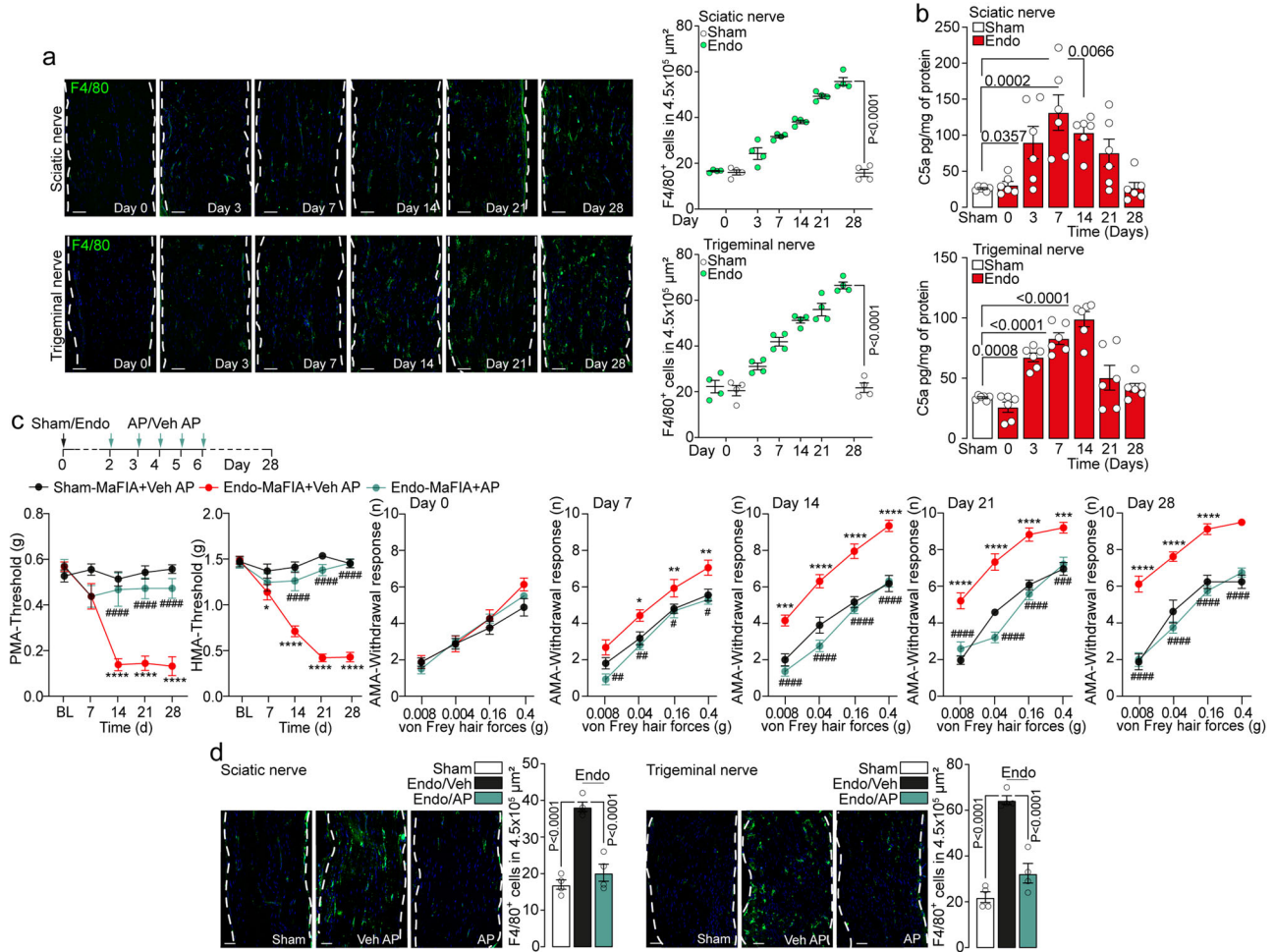


Fig. 2 | Neuroinflammation mediates endometriosis-associated mechanical allodynia. **a** Representative images and cumulative data of the time-dependent increase of F4/80⁺ cells in sciatic and trigeminal nerve in endometriotic (endo) or Sham C57BL/6J female (B6) mice. (*n* = 4 independent experiments). **b** Time-dependent C5a levels in sciatic and trigeminal nerve homogenates from endo and Sham B6 mice. (*n* = 6 independent experiments). **c** Timeline of the AP20187 (AP) treatment schedule and time-dependent periorbital (PMA), hind paw (HMA) and abdominal (AMA) mechanical allodynia in endo and Sham MaFIA mice after

intraperitoneal (i.p.) injection of AP or vehicle (Veh). (*n* = 8 mice per group). **d** Representative images and cumulative data of F4/80⁺ cells in sciatic and trigeminal nerve of endo B6 mice after AP or Veh and in Sham mice (treatment schedule as in **b**). (*n* = 4 independent experiments). (Scale bar, 50 μm, dashed lines, *perineurium*). Data are mean ± s.e.m. **a**, **b**, **d** 1-way ANOVA, **c** 2-way ANOVA, Bonferroni correction; **P* < 0.05, ***P* < 0.01, ****P* < 0.001, *****P* < 0.0001 vs. Sham, #####*P* < 0.0001 vs. Endo-MaFIA+ Veh AP. Source data are provided as a Source Data file.

endometriosis. Immunofluorescent staining analysis of mouse sciatic and trigeminal nerve tissues revealed that C5aR1 staining was present in 92.2% ± 1.1 and 93.3% ± 0.44 of nucleated cells, respectively (Supplementary Fig. 3a). SCs, which represent 45.1% of the nucleated cells in mouse peripheral nerve tissues³⁷, were identified by SOX10 expression. Immunofluorescent staining analysis in mouse sciatic and mouse trigeminal nerves revealed that all SOX10⁺ cells co-express C5aR1 (Fig. 3a, b and Supplementary Fig. 3b). Expression of *C5aR1* mRNA was established in cultured mouse and human SCs by qRT-PCR assay (Fig. 3c). RNAscope assay revealed that the *C5aR1* mRNA expression in SOX10⁺ cells was not modulated in peripheral nerve tissue of endometriotic compared to Sham mice (Supplementary Fig. 3c).

To investigate the role of Schwann cell C5aR1 in mechanical allodynia, we used a *Plp^{Cre}* driver that functions as a lineage tracer to express a short hairpin RNA (shRNA) for selective silencing of C5aR1 in SCs by the injection of a Cre-dependent adeno-associated viral vector (AAV). A virus packaged with the AAVrh10 serotype for efficient infection of SCs was used with a *loxP*-flanked shRNA to express shRNA in SCs (AAV-*C5aR1*) (Fig. 3d). The efficacy of the gene silencing was evaluated in sciatic and trigeminal nerves by immunofluorescent

staining with the use of two different C5aR1 antibodies and by RT-qPCR in SCs isolated from peripheral nerve trunks (Fig. 3e, Supplementary Fig. 3d, e). The role of macrophage C5aR1 is well documented in different diseases^{38–40}. To confirm SC selective C5aR1 silencing, we evaluated the co-expression of F4/80 and C5aR1 in peripheral nerves of *Plp*-AAV-*C5aR1* and Control mice (Supplementary Fig. 3f). Systemic (intravenous, i.v.) administration of AAV-*C5aR1* attenuated endometriosis-induced PMA, HMA, AMA, and abdominal licking (Fig. 3f, Supplementary Fig. 3g) and macrophage increase in sciatic and trigeminal nerves in *Plp^{Cre}* but not in Control mice (Fig. 3g). To further investigate the ability of C5a to stimulate cultured mouse and human SCs to recruit macrophages, we used the Boyden chamber assay. Human and mouse SCs stimulated with C5a promoted macrophage migration through the microporous membrane that was inhibited in the presence of DF2593A (Fig. 3h).

Previous data reported *C5aR1* mRNA expression in mouse DRG neurons where C5a, by activating and sensitizing cutaneous nociceptors, amplified the capsaicin response⁴¹. To identify the role for neuronal C5aR1 in endometriotic pain, we used a *Adv^{Cre}* driver to silence C5aR1 selectively in sensory neurons and a virus packaged with the AAV2/9n serotype for efficient infection of nociceptors. Selective

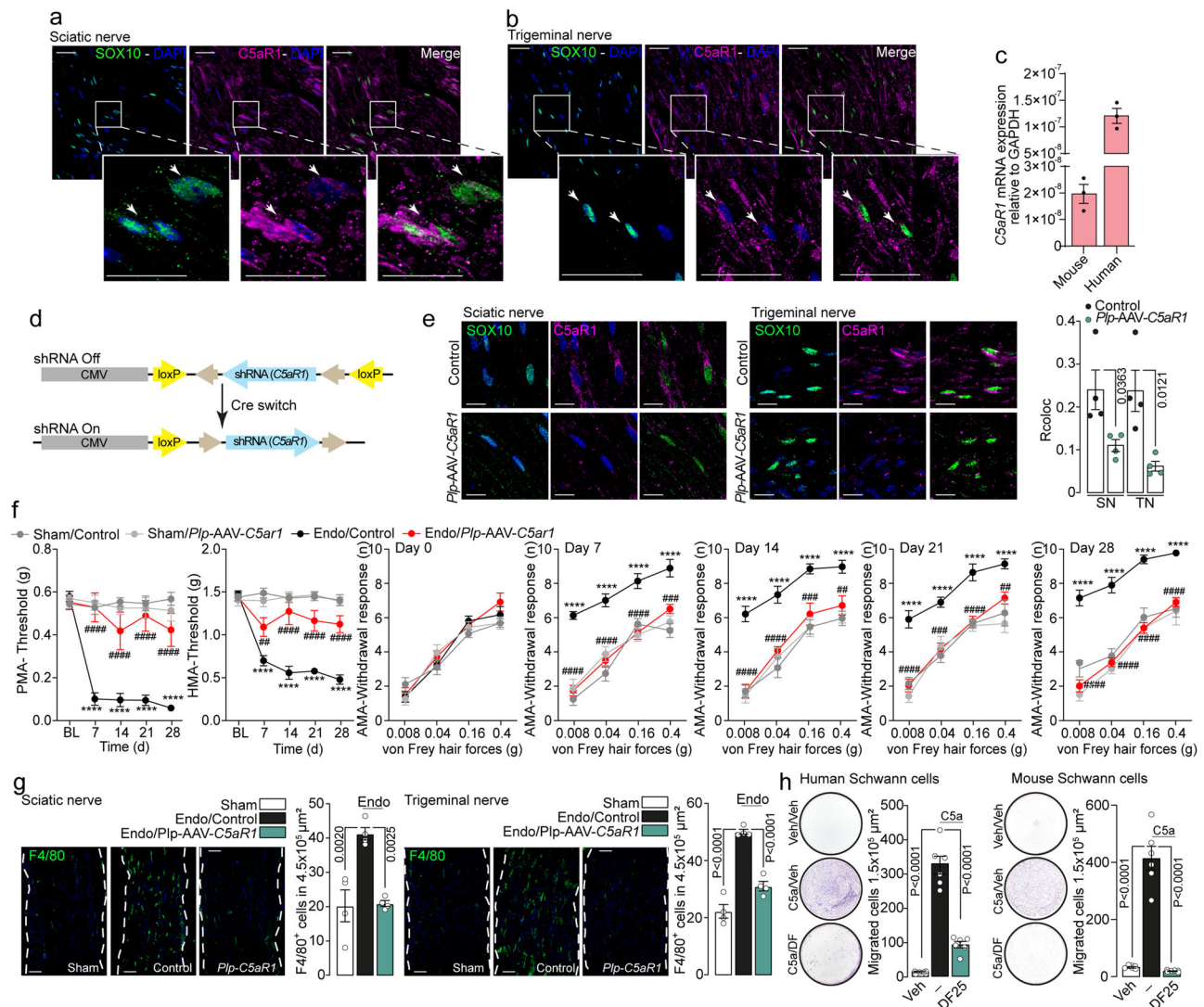


Fig. 3 | Schwann cell C5aR1 mediates endometriosis-associated mechanical allodynia and neuroinflammation. Representative images of SOX10 and C5aR1 (#orb393229, rabbit polyclonal, Biorbyt Ltd, 1:100) co-expression in sciatic (a) and trigeminal (b) nerve tissue from C57BL/6J female (B6) mice, ($n = 4$ independent experiments) (Scale bar, 50 μm). (c) C5aR1 mRNA relative expression in primary mouse and human Schwann cells ($n = 3$ independent experiments). (d) Schematic representation of AAV-(loxP-shRNA)-C5aR1 vector pre- and post-Cre switch. (e) Representative images and cumulative data (Rcoloc) of SOX10 and C5aR1 (#orb393229, rabbit polyclonal, Biorbyt Ltd, 1:100) co-expression in sciatic and trigeminal nerve tissue in Pfp-AAV-C5aR1 and Control mice ($n = 4$ independent experiments) (Scale bar, 50 μm). (f) Time-dependent periorbital (PMA), hind paw

(HMA), and abdominal (AMA) mechanical allodynia in endometriotic (endo) or Sham Pfp-AAV-C5aR1 and Control mice. ($n = 8$ mice per group). (g) Representative images and cumulative data of F4/80⁺ cells in sciatic and trigeminal nerve tissue in endo or Sham Pfp-AAV-C5aR1 and Control mice. ($n = 4$ independent experiments) (Scale bar, 50 μm , dashed lines, *perineurium*). (h) Representative images and cumulative data of transmigrated macrophages after stimulation of human and mouse Schwann cells with C5a or vehicle (Veh) and in the presence of DF2593A (DF25) or Veh ($n = 6$ independent experiments). Data are mean \pm s.e.m. (c, Student's *t*-test, (f, 2-way, (g, h) 1-way ANOVA, Bonferroni correction; **** $P < 0.0001$ vs. Sham/Control, **** $P < 0.0001$ vs. Endo/Control. Source data are provided as a Source Data file.

silencing of C5aR1 in sensory neurons was confirmed by immunofluorescent staining in lumbar (L4-L6) dorsal root ganglion (DRG) tissues (Supplementary Fig. 3h). Intrathecal administration of AAV-C5aR1 in *Adv^{Cre}* did not attenuate endometriosis-induced PMA, HMA, and AMA and macrophage increases in nerve (sciatic and trigeminal) trunks (Supplementary Fig. 3i,j). These results indicate that, in endometriotic mice, C5a targeting of the SC C5aR1 is necessary and sufficient to induce neuroinflammation and mechanical allodynia.

Schwann cell NLRP1 drives endometriosis-induced macrophage increases and mechanical allodynia

C5aR1 is known to activate the NLR family pyrin domain containing 3 (NLRP3) inflammasome, thus promoting the expression of the interleukin-1 β precursor (pro-IL-1 β) and secretion of IL-1 β through the

cleavage by caspase-1 in different immune cells⁴². Here, we report that human SC C5aR1 encoded a signaling pathway that released IL-1 β , a response attenuated by the C5aR1 inhibitor, DF2593A (Fig. 4a). IL-1 β plasma levels from endometriotic mice were more elevated from day 10 until day 28 after surgery as compared to sham mice (Fig. 4b). Increased IL-1 β plasma levels were also detected in women with endometriosis as compared to healthy women without endometriosis (Fig. 4c). To assess caspase-1 activation, cultured human SCs were exposed to C5a that increased a bioluminescent signal due to caspase-1 activation. The increase was reduced by DF2593A and by the selective caspase-1 inhibitor, Ac-YVAD-CHO (Supplementary Fig. 4a). Further support to caspase-1 activation was obtained by genetically encoded fluorescent sensor (SCAT1) based on fluorescence resonance energy transfer (FRET)⁴³. SCAT1 contains a consensus peptide preferentially

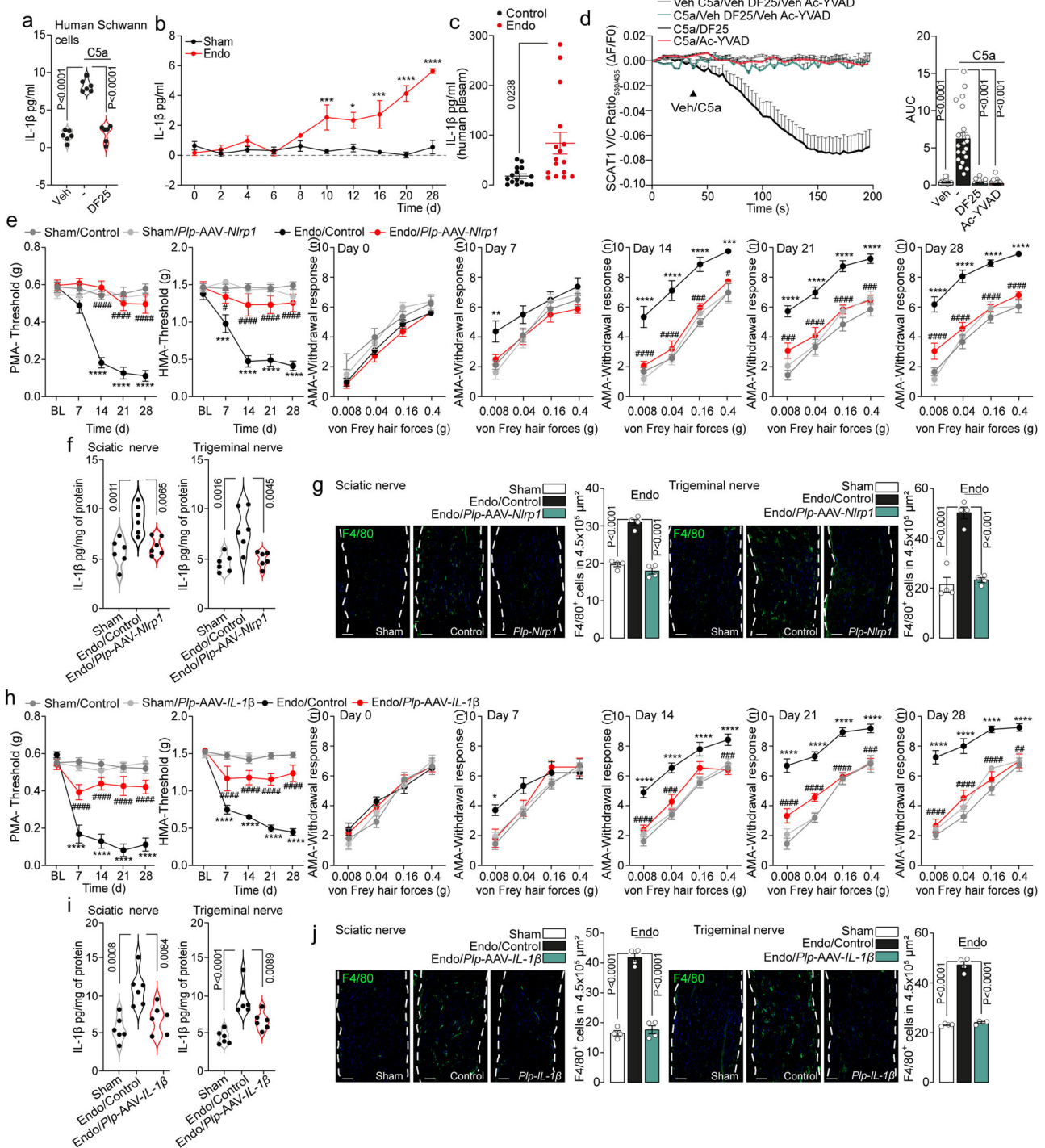


Fig. 4 | Schwann cell C5aR1 activation induces NLRP1-dependent release of IL-1β. **a** IL-1β assay in human Schwann cell conditioned medium after stimulation with C5a or vehicle (Veh) and in the presence of DF2593A (DF25) or Veh ($n = 6$ independent experiments). **b** Time-dependent C5a levels in plasma samples from endometriotic (endo) or Sham C57BL/6J female (B6) mice. ($n = 8$ independent experiments). **c** IL-1β assay in plasma samples from endo patients ($n = 16$) or healthy subjects ($n = 15$) (control). **d** Typical traces and cumulative data of SCAT1 V/C ratio changes in human Schwann cells stimulated with C5a or Veh and in the presence of DF25 or Ac-YVAD (AUC, area under the curve) (cell numbers: C5a = 20, Veh = 16, DF25 = 16 and Ac-YVAD = 20; $n = 3$ independent experiments) **e** Time-dependent periorbital (PMA), hind paw (HMA) and abdominal (AMA) mechanical allodynia in endo or Sham *Plp-AAV-Nlrp1* and Control mice ($n = 8$ mice per group). **f** IL-1β assay in sciatic and trigeminal nerve tissue homogenates in endo or Sham *Plp-AAV-Nlrp1*

and Control mice ($n = 6$ independent experiments). **g** Representative images and cumulative data of F4/80⁺ cells in sciatic and trigeminal nerves in endo or Sham *Plp-AAV-Nlrp1* and Control mice ($n = 4$ independent experiments). **h** Time-dependent PMA, HMA, and AMA in endo or Sham *Plp-AAV-IL-1β* and Control mice ($n = 8$ mice per group). **i** IL-1β assay in sciatic and trigeminal nerve tissue homogenates in endo or Sham *Plp-AAV-IL-1β* and Control mice. **j** Representative images and cumulative data of F4/80⁺ cells in sciatic and periorbital nerve in endo or Sham *Plp-AAV-IL-1β* and Control mice (Scale bar, 50 μm, dashed lines, *perineurium*) ($n = 8$ mice per group). Data are mean ± s.e.m. **a, c, d, f, g** 1-way ANOVA, **b, e, h** 2-way ANOVA, Bonferroni correction; * $P < 0.05$, ** $P < 0.01$, *** $P < 0.001$, **** $P < 0.0001$ vs. Sham, # $P < 0.05$, ## $P < 0.01$, ### $P < 0.001$, #### $P < 0.0001$ vs. Endo/Control. Source data are provided as a Source Data file.

cleaved by caspase-1 that reduces the FRET signal⁴³. C5a decreased SCAT1 Venus/ECFP (V/C) ratio, a response that was prevented by DF2593A and Ac-YVAD-CHO in human SCs (Fig. 4d). Ac-YVAD-CHO inhibited the release of IL-1 β from human SCs after C5a stimulation, supporting the role of C5aR1 in promoting inflammasome activation and IL-1 β release (Supplementary Fig. 4b).

Endometriotic mice with AAV-mediated selective silencing of C5aR1 (*Plp-AAV-C5aR1* mice) showed reduced levels of IL-1 β in sciatic and trigeminal nerve tissues compared to Control mice (Supplementary Fig. 4c). To test the role of SC NLRP3 in endometriotic mechanical allodynia, we injected *Plp^{Cre}* mice with an AAV-*Nlrp3* for selective silencing of NLRP3 in SCs (*Plp-AAV-Nlrp3* mice). However, PMA, HMA, AMA, abdominal licking, neuroinflammation, and IL-1 β levels in sciatic and trigeminal nerve tissue in endometriotic *Plp-AAV-Nlrp3* mice were unaffected (Supplementary Fig. 4d-h). The efficacy of the gene silencing was evaluated in sciatic and trigeminal nerve tissue by immunofluorescent staining and by RT-qPCR in SCs isolated from peripheral nerve trunks (Supplementary Fig. 4i, j).

The inflammasome family currently includes three subtypes, NLRP1, NLRP3, and NLRC4, which recognize specific classes of pathogens or risk signals⁴⁴. The qRT-PCR analysis of mRNA expression in both human and mouse SCs revealed mainly the presence of *Nlrp1* and *Nlrp3* transcripts (Supplementary Fig. 4k). Given the very low level of *Nlrp4* expression, we tested the role of SC NLRP1 in endometriotic pain by infecting *Plp^{Cre}* mice with an AAV-*Nlrp1* for selective silencing of NLRP1 in SCs (*Plp-AAV-Nlrp1*). *Plp-AAV-Nlrp1* mice showed reduced PMA, HMA, AMA, abdominal licking, IL-1 β levels and neuroinflammation in sciatic and trigeminal nerve tissue compared to Control mice (Fig. 4e-g, Supplementary Fig. 4l). The efficacy of NLRP1 gene silencing was evaluated in sciatic and periorbital nerve tissue by immunofluorescent staining and in peripheral nerve isolated SCs by RT-qPCR (Supplementary Fig. 4m, n). Quantification of *Nlrp3* and *Nlrp1* transcript levels in sciatic and periorbital nerve tissues from endometriotic and Sham B6 mice excluded that endometriosis modulates mRNA (Supplementary Fig. 4o).

Previous studies indicated a crucial role of IL-1 β in sustaining inflammation through macrophage recruitment⁴⁵. To support the role of IL-1 β in increasing macrophage number in nerve trunks, mouse and human SCs and macrophages were exposed to a neutralizing monoclonal antibody against IL-1 β (anti-IL-1 β mAb) or C5a in a Boyden chamber assay. The anti-IL-1 β mAb reduced macrophage migration evoked by C5a (Supplementary Fig. 5a). The anti-IL-1 β mAb treatment also reduced PMA, HMA, and AMA and macrophage numbers in sciatic and trigeminal nerves in endometriotic mice (Supplementary Fig. 5b,c). To identify the SC role in releasing IL-1 β following C5a stimulation in endometriotic mice, we selectively silenced IL-1 β in SCs by infecting *Plp^{Cre}* mice with an AAV-*IL-1 β* (*Plp-AAV-IL-1 β* mice). *Plp-AAV-IL-1 β* mice showed reduced PMA, HMA, AMA, abdominal licking (Fig. 4h, Supplementary Fig. 5d), IL-1 β levels (Fig. 4i), and neuroinflammation in sciatic and trigeminal nerve tissue (Fig. 4j) compared to Control mice. The efficiency of gene silencing was evaluated in sciatic and trigeminal nerve tissue by immunofluorescent staining (Supplementary Fig. 5e). Overall, these data support the view that C5a from endometriotic lesions targets SC C5aR1, which activates inflammasome NLRP1 to release IL-1 β , which in turn increases macrophages within peripheral nerve trunks to sustain mechanical allodynia.

Non-neuronal TRPA1 mediates endometriosis-induced neuroinflammation that engages the neuronal TRPA1 to signal pain

We previously reported that oxidative stress generated by macrophages recruited at sites of nerve injury targets SC TRPA1 to amplify the local oxidative burden that eventually engages the SC TRPA1 to sustain neuroinflammation and the neuronal TRPA1 to signal pain in several mouse models^{26-28,46}. Here, we confirm that the time-dependent F4/80+ cell increase in sciatic and trigeminal nerves of

endometriotic mice (Fig. 2a) was associated with augmented oxidative stress byproduct 4-hydroxynonenal (4HNE) (Supplementary Fig. 6a). Selective silencing of SC *C5aR1*, *Nlrp1* or *IL-1 β* in *Plp-AAV-C5aR1*, *Plp-AAV-Nlrp1* or *Plp-AAV-IL-1 β* mice, respectively, prevented the accumulation of 4-HNE in peripheral nerves of endometriotic mice (Supplementary Fig. 6b).

To show the role of SC TRPA1 as sensor and amplifier of the oxidative stress that sustains neuroinflammation and pain and of neuronal TRPA1 to sustain pain, we used *Plp^{Cre}* and *Adv^{Cre}* mice with selective deletion of TRPA1 in SCs (*Plp-Trpa1*) and DRG neurons (*Adv-Trpa1*), respectively. Whereas PMA, HMA, and AMA induced by endometriosis were reduced in both *Plp-Trpa1* and *Adv-Trpa1* mice, neuroinflammation (macrophages and 4-HNE) was attenuated only in *Plp-TRPA1* endometriotic mice (Fig. 5a-f). These data confirm that non-neuronal TRPA1 maintains the proinflammatory condition, while neuronal TRPA1 is the final common pathway that, from endometriotic lesions and via SCs, signals mechanical allodynia.

Discussion

Here, we provide evidence that, in the present mouse model of endometriosis, peritoneal lesions, by increasing serum levels of C5a, not only increase neuronal sensitivity in local mesenteric nociceptors, but also promote a macrophage-dependent proalgesic mechanism that spreads throughout the body, reaching distant anatomical regions, including the periorbital or hind paw areas. We reveal that C5a, in both proximal and remote areas, such as the abdomen and periorbital area/hind paw, respectively, targets the SC C5aR1, where it encodes a proalgesic mechanism that results in neuroinflammation and the ensuing widespread mechanical allodynia. Another unexpected finding of the present study highlights the role of the inflammasome NLRP1, instead of the classical NLRP3, normally activated by C5a, as we found that SC C5aR1 via NLRP1 enhances the caspase-1 processing of pro-IL-1 β . The resulting IL-1 β release increases the macrophage number that, via their oxidative burst targets SC TRPA1 and en route neuronal TRPA1, to sustain mechanical allodynia.

C5a has been implicated in various pain conditions, including post-operative¹⁷, inflammatory¹⁸, and neuropathic pain²⁵. Although little is known about the association between the complement system components and endometriotic pain, fluctuation of C5a plasma levels during the different stages of the disease has been documented in endometriosis patients^{21,47}, an observation that we confirmed here. Time course analysis of C5a plasma levels in the present mouse model of endometriosis showed similar fluctuations in female mice with endometriotic lesions, which were identified as the initial stimulus responsible for the abdominal and diffuse proalgesic condition.

A considerable proportion of women with endometriosis-associated pain reported a neuropathic-like pain component⁴⁸. Recently, it has been observed that neuropathic-like pain caused by peripheral nerve injury in mice was modulated by activation of neuron-associated C5aR1+ macrophages²⁵. Present results with the C5aR1 inhibitor and transgenic MaFIA mice confirm that increases in plasma C5a and nerve trunk macrophages are essential for the development of endometriosis-associated pain-like responses. We also found that endometriotic lesions promote mechanical allodynia in various and distant tissues by orchestrating a series of temporally distinct but strictly coordinated phases. The role of C5a was confined to its initial sharp increase. Although C5aR1 expression has not been reported in SCs located at neuromuscular junctions³⁹, we found that both cultured primary human and mouse SCs and SOX10+ cells in mouse and human peripheral nerve fibers expressed C5aR1. By C5aR1 selective silencing, we highlighted the role of SC C5aR1 in endometriosis-associated mechanical allodynia and neuroinflammation.

Recent studies suggest that the C5a-C5aR1/C5aR2 interaction regulates the NLRP3 inflammasome in several immune system cells, including macrophages^{49,50} and T cells⁵¹. Furthermore, NLRP3 has been

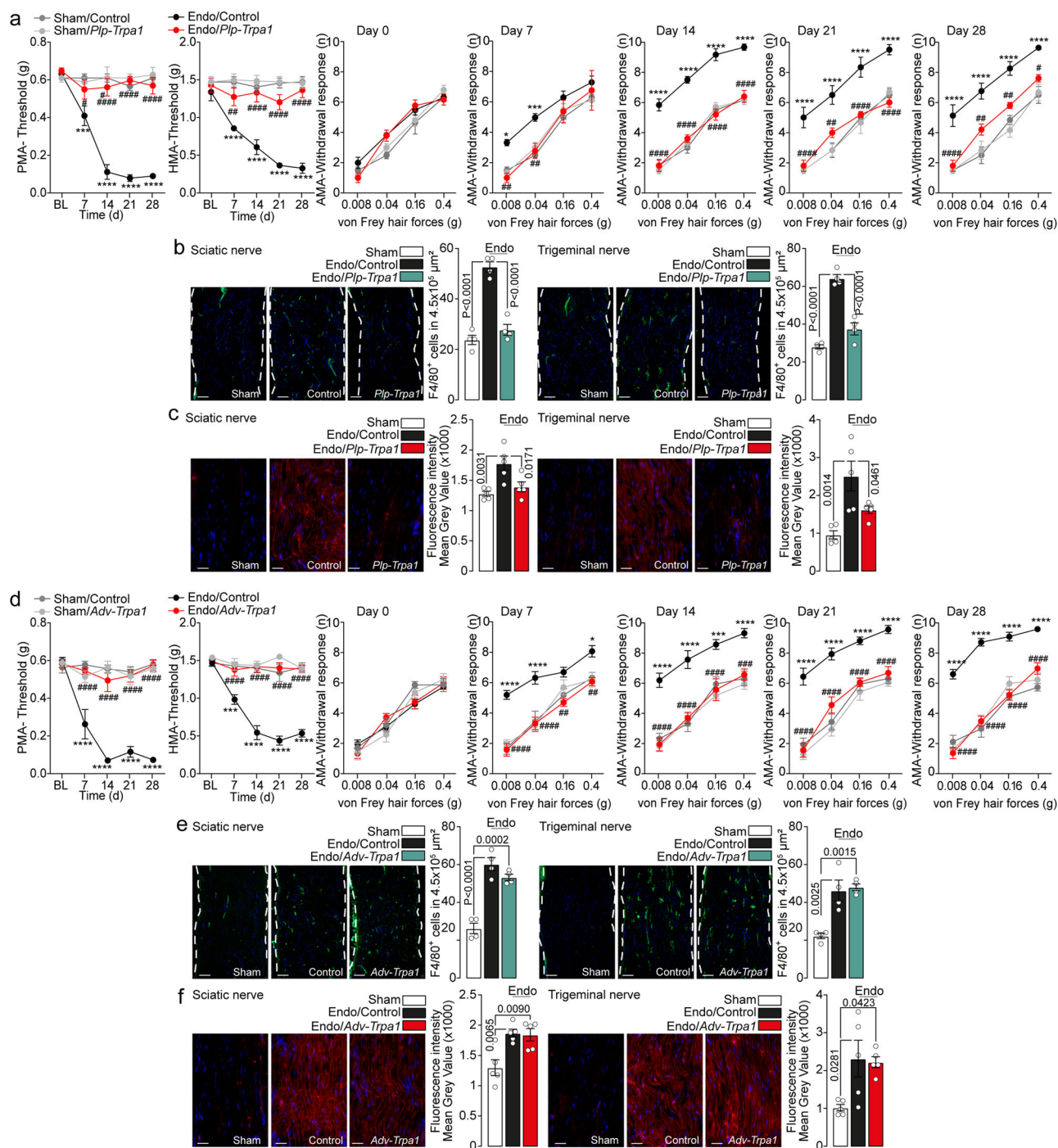


Fig. 5 | Schwann cell TRPA1 channel mediates endometriosis-associated mechanical allodynia and neuroinflammation. **a** Time-dependent periorbital (PMA), hind paw (HMA) and abdominal (AMA) mechanical allodynia in endometriotic (endo) or Sham *Plp-Trpa1* and Control mice ($n = 8$ mice per group). Representative images and cumulative data of **(b)** F4/80⁺ cells and **(c)** 4-HNE staining in sciatic and trigeminal nerve in endo or Sham *Plp-Trpa1* and Control mice (Scale bar, 50 μm, dashed lines, *perineurium*) ($n = 4$ and $n = 5$ independent experiments). **d** Time-dependent PMA, HMA and AMA in endometriotic (endo) or Sham *Adv-*

Trpa1 and Control mice ($n = 8$ mice per group). Representative images and cumulative data of **(e)** F4/80⁺ cells and **(f)** 4-HNE staining in sciatic and trigeminal nerve in endo or Sham *Adv-Trpa1* and Control mice (Scale bar, 50 μm, dashed lines, *perineurium*) ($n = 4$ independent experiments). Data are mean \pm s.e.m. **a, d** 2-way ANOVA, **b, c, e, f** 1-way ANOVA, Bonferroni correction; * $P < 0.05$, *** $P < 0.001$, **** $P < 0.0001$ vs. Sham, # $P < 0.05$, ## $P < 0.01$, ### $P < 0.001$, #### $P < 0.0001$ vs. Endo/Control. Source data are provided as a Source Data file.

implicated in the pathobiology of chronic neuropathic and inflammatory pain^{52–54}. Inflammation is one of the key features of endometriosis, and the inhibition of NLRP3 inflammasome has been associated with the reduction of IL-1 β secretion from endometrial stromal cells^{35,56} and mast cells⁵⁷. However, the present observation that selective silencing in SCs of the NRLP3 subtype in endometriotic mice was

ineffective, whereas silencing of the NRLP1 SC subtype reduced IL-1 β release and mechanical allodynia, implicates NRLP1 in the proalgesic pathway promoted by endometriosis.

The time course of the various soluble and cellular mediators involved in endometriosis-induced mechanical allodynia is under a strict sequential order, as it encompasses the contribution of at least

three different cell subtypes, macrophages, DRG neurons and, with a key role, SCs. The transient (from day 2 to day 8 post-surgery) increase in C5a plasma levels, which targets the SC C5aR1 is the initial step. C5aR1 encodes an intracellular signaling pathway that encompasses NLRP1-dependent caspase-1 activation and the ensuing cleavage of pro IL-1 β to release IL-1 β . IL-1 β increases macrophages within the nerve trunks. Macrophages, as shown in other pain mouse models^{26–28}, via their oxidative burst, activate the SCs TRPA1 that by amplifying ROS production sustain neuroinflammation and by targeting neuronal TRPA1 signal pain. A limitation of the present study is that we did not further explore additional downstream and upstream factors that might be implicated in the proalgesic C5a/IL-1 β pathway in endometriosis.

The role of C5a as a soluble and diffusible pain mediator explains the epidemiological observation that other painful conditions, like migraine or fibromyalgia, coexist with endometriosis^{7,8,10,58}. The C5aR1 expression in SCs where it promotes mechanical allodynia and neuroinflammation may explain how endometriosis features chronic pain as a major symptom of the disease. A second limitation of our study is that we documented all the cellular and molecular steps of the endometriotic inflammatory and proalgesic pathways in sciatic and trigeminal nerve trunks, implicated in fibromyalgia and migraine pain, respectively, but in contrast, due to the limited size of mesenteric nerve fibers, we could not assess these cellular and molecular steps underlying mechanical allodynia in the abdomen, the primary site of endometriotic pain. However, functional experiments in mice with selective silencing in SCs suggest that abdominal mechanical allodynia is produced by the same mechanisms identified in sciatic and trigeminal nerves. Therapies targeted to the cellular and molecular mediators of the C5a-C5aR1/NLRP1/IL-1 β pathway in SCs may be future options for the treatment of pain in endometriosis patients.

Methods

The research conducted complies with all relevant ethical regulations. All behavioral experiments followed Animal Research: Reporting of In Vivo Experiments (ARRIVE) guidelines and were in accordance with European Union (EU) guidelines for animal care procedures and the Italian legislation (DLgs 26/2014) application of the EU Directive 2010/63/EU. The study was approved by the National Committee for the Protection of Animals used for Scientific Purposes of the Italian Ministry of Health (research permits # 452/2020-PR).

The use of blood plasma samples collected from human individuals (female) diagnosed with endometriosis and healthy control (female) was approved by the Local Ethics Committee of the Florence University Hospital (Area Vasta Toscana Centro, CEAVC) (EndoTRP study, 1521Loss and subsequent amendments), according to the Helsinki Declaration and good clinical practice guidelines, and all patients gave their informed consent. Participants did not receive any form of compensation. The blood plasma samples derived from nineteen endometriosis-diagnosed patients [female, median age 30 years (range 22–43)] and fifteen healthy individuals [female, median age 27 years (23–42)]. Female patients were enrolled as endometriosis is a gynaecological condition. Sex of the participants was self-determined. Considering the exploratory nature of the blood sampling analyses, the sample size was not determined based on statistical considerations but enrolling all consecutive outpatients and healthy controls.

Experimental model and content details

Animals. Female mice were used throughout (25–30 g, 6–8 weeks old). The following strains of mice were used: C57BL/6J (Charles River, RRID: IMSR_JAX:000664), B6.Cg-Tg(Plp1-CreERT)3Pop/J mice (*Plp-Cre^{ERT}*, RRID: IMSR_JAX:005975 Jackson Laboratory) expressing a tamoxifen-inducible Cre in Schwann cells (Plp1, proteolipid protein myelin 1). Both positive and negative mice for *Cre^{ERT}* (*Plp-Cre^{ERT+}* or *Plp-Cre^{ERT-}* (control) respectively) were treated with intraperitoneal (i.p.)

4-hydroxytamoxifen (4-OHT, 1 mg/100 μ L in corn oil once a day consecutively for 3 days) before the infection with AAV for selective silencing of the different genes in Schwann cells. To generate mice in which the *Trpa1* gene was conditionally silenced in Schwann cells, homozygous 129S-*Trpa1^{tm2Kykwl}* (floxed *Trpa1*, *Trpa1^{flox}*, RRID:IMSR_JAX:008649 Jackson Laboratory) were crossed with hemizygous B6.Cg-Tg(Plp1-CreERT)3Pop/J mice (*Plp-Cre^{ERT}*, RRID: IMSR_JAX:005975 Jackson Laboratory)²⁶. The progeny (*Plp-Cre^{ERT};Trpa1^{flox}*) was genotyped using PCR for *Trpa1* and *Plp-Cre^{ERT}*. Mice that were negative for *Plp1-Cre^{ERT}* were used as controls. Both positive and negative mice for *Cre^{ERT}* and homozygous floxed *Trpa1* (*Plp-Trpa1* and control, respectively) were treated with i.p. 4-OHT (1 mg/100 μ L in corn oil) once a day consecutively for 3 d. This treatment resulted in the Cre-mediated ablation of *Trpa1* in Schwann cells expressing Plp. To selectively delete *Trpa1* in primary sensory neurons, homozygous 129S-*Trpa1^{tm2Kykwl}* (floxed *Trpa1*, *Trpa1^{flox}*, RRID:IMSR_JAX: 008649 Jackson Laboratory) mice were crossed with hemizygous Advillin-Cre mice (*Adv-Cre*). Mice positive or negative for Cre and homozygous for floxed *Trpa1* (*Adv-Trpa1* and control, respectively) were used. The successful Cre-driven deletion of *Trpa1* mRNA was confirmed using reverse transcription quantitative real-time PCR (RT-qPCR). Some *Adv-Cre⁺* or *Adv-Cre* (control) were used for the infection with AAV for selective gene silencing in primary sensory neurons.

To evaluate the involvement of macrophages, transgenic Macrophage Fas-Induced Apoptosis (MaFia) mice (C57BL/6-Tg(Csflr-EGFP-NGFR/FKBP1A/TNFRSF6)2Bck/J, stock No: 005070, RRID:IMSR_JAX:005070, Jackson Laboratories) were used. These transgenic mice express a mutant human FK506 binding protein 1A, 12 kDa (FKBP12)-Fas inducible suicide/apoptotic system, driven by the mouse Csflr promoter conjugated with a green fluorescent protein (GFP), which preferentially binds the B/B dimerizing agent (B/B-HmD, AP20187). Treatment of mice with AP20187 induces the dimerization of the suicide protein to activate the cytoplasmic FKBP12-Fas fragments, leading to the apoptosis of transgene-expressing cells and consequent macrophage depletion³⁵.

The group size of $n = 8$ mice for behavioral experiments was determined by sample size estimation using G Power [v3.1⁵⁹] to detect the size effect in a *post-hoc* test with type 1 and 2 error rates of 5% and 20%, respectively. Allocation concealment of mice into the vehicle(s) or treatment groups was performed using a randomization procedure (<http://www.randomizer.org/>). The assessors were blinded to the identity of the animals (genetic background) or allocation to treatment groups. None of the animals were excluded from the study. Mice were housed in a temperature ($20 \pm 2^\circ\text{C}$) and humidity ($50 \pm 10\%$) controlled vivarium [12 h dark/light cycle, free access to food (#2018 Teklad Global 18% Protein Rodent Diet, Envigo) and water, five animals per cage]. At least 1 h before behavioral experiments, mice were acclimatized to the experimental room and behavior was evaluated between 9:00 am and 5:00 pm. Animals were anesthetized with a mixture of ketamine and xylazine (90 mg/kg and 3 mg/kg, respectively, i.p.) and euthanized with inhaled CO₂ plus 10–50% O₂.

Cell lines

Mouse Schwann cells (MSC). MSC were isolated from sciatic nerves of C57BL/6J mice⁶⁰, *Plp-AAV-C5aR1*, *Plp-AAV-Nlrp1*, *Plp-AAV-Nlrp3* and Control mice. Briefly, the epineurium was removed, and nerve explants were cut into 1 mm segments and enzyme-dissociated in Hank's Balanced Salt Solution (HBSS, 2 hr, 37 $^\circ\text{C}$) added with collagenase (0.05%) and hyaluronidase (0.1%). Cells were collected by centrifugation (150xg, 10 min, room temperature, RT) and the pellet was resuspended and cultured in Dulbecco's Modified Eagle Medium (DMEM) containing fetal calf serum (10%), L-glutamine (2 mM), penicillin (100 U/ml), streptomycin (100 mg/ml), neuregulin (10 nM) and forskolin (2 μ M). Cytosine arabinoside (Ara-C, 10 mM) was added three days later, to remove fibroblasts. The culture medium was replaced

every 3 days. Cells were cultured at 37 °C in 5% CO₂ and 95% O₂ for 15 days before experiments.

Human Schwann cells (HSCs). HSCs (#P10351; Innoprot) were grown in Schwann cell medium (#P60123, Innoprot) at 37 °C with 5% CO₂ and 95% O₂ and discarded and replaced after 12 passages⁴⁶.

The murine macrophage cell lineage, RAW 264.7 (#TIB-71™; ATCC, RRID: CVCL_0493), was cultured and maintained in DMEM supplemented with FBS (10%), penicillin (100 U/mL), streptomycin (100 mg/mL) and L-glutamine (2 mM) at 37 °C in 5% CO₂ and 95% O₂.

The human monocytic cell line, U937 (#CRL-1593.2™; ATCC, RRID:CVCL_0007) was maintained at 37 °C, 5% CO₂ and 95% O₂ in Roswell Park Memorial Institute (RPMI-1640) medium supplemented with heat-inactivated FBS (10%), L-glutamine (2 mM), 4-(2-hydroxyethyl)-1-piperazineethanesulfonic acid (HEPES; 10 mM), and sodium pyruvate (1 mM). The differentiation of U937 cells (1 × 10⁵ cells/mL) towards macrophage-like lineage was promoted by the exposure to 200 ng/mL of phorbol 12-myristate 13-acetate (PMA) for 2 days before experiments⁶¹.

AAVpro293T cell line. AAVpro 293T cells (#632273, Takara, RRID:CVCL_BOXW), were maintained in DMEM high glucose supplemented with 10% heat inactivated FBS, 4 mM L-glutamine, 1 mM penicillin/streptomycin and 1 mM sodium pyruvate at 37 °C in 5% CO₂ and 95% O₂. The day before transfection, cells were plated in DMEM supplemented with 2% FBS.

Human embryonic kidney 293 T (HEK 293 T) cell line. HEK 293 T cells (#CRL-3216, ATCC, RRID:CVCL_0063) were maintained in DMEM high glucose supplemented with 10% heat inactivated FBS, 2 mM L-Glutamine and 1 mM penicillin/streptomycin at 37 °C in 5% CO₂ and 95% O₂ before transfection.

HEK293T cells transfection

HEK293T cells were plated on poly L-lysine-coated (8.3 μM) 35-mm glass coverslips and maintained at 37 °C in 5% CO₂ and 95% O₂ 16 h before transfection. Cells were transfected with plasmid DNA (2 μg) expressing murine *C5aRI* (#MR223830, Origene), *Nlrp1a* (#MR221045, Origene), *Nlrp1b* (#MR215179, Origene) and *Nlrp3* (#75127, Addgene) genes using jetOPTIMUS® DNA transfection reagent (#55-250; Polyplus, Lexington, MA, USA) and incubated for 24 h before immunofluorescence.

Induction of endometriosis

Endometriosis was induced in mice as previously reported⁶². Briefly, donor mice, received a subcutaneous injection of estradiol benzoate (3 μg/100 μL) to stimulate the endometrium growth. Seven days later, the uteri of the donor mice were dissected and divided longitudinally. Uterine horns from each donor mouse were minced in tissue fragment smaller than 1 mm in Hank's balanced salt solution (HBSS). Each dissociated uterine horn was then injected intraperitoneally (50 mg/500 μL i.p.) in recipient mice. One donor mouse was used for every 2 endometriosis mice. Sham mice received an intraperitoneal injection of 500 μL of HBSS. Behavioral experiments were performed during a 28-day period. After 28 days from the injection of the endometrium suspension, mice were sacrificed, and tissues collected. Lesion implantation was also quantified in a time-course manner by counting the number of lesions in endometriotic mice at day 7, 14, 21, and 28.

Treatment protocols

If not otherwise indicated, all reagents were obtained from Merck Life Science SRL. Mice received systemic administration of C5a complement antagonist (DF2593A, 1 mg/kg, intragastric, i.g.) or vehicle (0.5% carboxymethyl cellulose, CMC) twice a day, by two different time

schedules: from one day before the endometriotic tissue injection to day 6 or from day 12 to day 16.

Anti-IL-1β (#BE02463, clone B122, Bio X Cell, RRID:AB_2687727) monoclonal antibody (mAb) or IgG isotype control were administered (50 μg/200 μL, i.p.) at day 8 and day 14 after endometriosis/sham induction. C6 antisense oligonucleotide (5'-AACTgtctgggAAT-3' where Locked Nucleic Acid are in capital letter and DNA in lowercase)³² (5 mg/kg, subcutaneous, s.c.) or vehicle (PBS) were injected once daily, from one day before the endometriotic tissue injection to day 6.

MaFIA mice were treated with B/B homodimerizer (AP20187, 2 mg/kg, i.p., once a day) or vehicle (10% PEG-400, 1.7% tween 80 in 0.9% NaCl) by three different time schedules: from day -2 to day 2; from day 2 to day 6, and from day 21 to day 25. *Plp-Cre*⁺ and control mice were infected with an intravenous (1 mL/kg, 1 × 10¹² v/g, i.v.) injection of different AAVs. *Adu-Cre*⁺ and control mice were infected with an intrathecal (1 × 10¹² v/g, i.th., 5 μL) injection of AAV. Animals were used 3 weeks after AAVs infection. Sciatic and trigeminal nerve tissues were harvested for evaluating AAVs infection.

Behavioral assays

Abdominal Mechanical allodynia (AMA). The mechanical pain sensitivity of the abdominal region was evaluated with von Frey filaments by methods described previously⁶³. Mice were habituated in small compartments on a perforated grid for 1 h before the test. Subsequently, von Frey filaments were applied to the abdomen (between diaphragm and genitals). The test was performed by a trained blinded observer. The individual filaments were tested in an ascending order covering 0.008, 0.04, 0.16, and 0.4 g forces. Each force was applied 10 times to the abdominal surface. The maximal duration of each force application was 2 s, and the inter-stimulus interval was 2–3 min. Following each challenge, the withdrawal response was quantified either as 1 (withdrawal of abdominal wall, licking or retraction of animal) or 0 (no response). All counts in response to an individual filament were averaged. Withdrawal responses to low forces reflect high mechanical pain sensitivity.

Periorbital mechanical allodynia (PMA). Periorbital mechanical allodynia (PMA) was assessed using the up-down paradigm^{64,65}. Briefly, mice were placed in a restraint apparatus designed for the evaluation of periorbital mechanical thresholds⁶⁶. PMA was evaluated in the periorbital region over the rostral portion of the eye (i.e., the area of the periorbital region facing the sphenoidal rostrum)⁶⁷ before (basal threshold) and after treatments. On the day of the experiment, after 20 min of adaptation inside the chamber, a series of 7 von Frey filaments in logarithmic increments of force (0.02, 0.04, 0.07, 0.16, 0.4, 0.6 and 1.0 g) were applied to the periorbital area perpendicular to the skin, with sufficient force to cause slight buckling, and held for approximately 5 s to elicit a positive response. The response was considered positive by the following criteria: mouse vigorously stroked its face with the forepaw, head withdrawal from the stimulus, or head shaking. Mechanical stimulation started with the 0.16 g filament. Absence of response after 5 s led to the use of a filament with increased force, whereas a positive response led to the use of a weaker (i.e., lighter) filament. Six measurements were collected for each mouse or until four consecutive positive or negative responses occurred. The 50% mechanical withdrawal threshold (expressed in g) was then calculated from these scores by using a δ value of 0.205, previously determined⁶⁷.

Hindpaw Mechanical allodynia (HMA). Paw mechanical allodynia was evaluated by measuring the paw withdrawal threshold by using the up-down paradigm^{64,68}. Mice were acclimatized (1 h) in individual clear plexiglass boxes on an elevated wire mesh platform, to allow for access to the plantar surfaces of the hind paws. von Frey filaments of increasing stiffness (0.07, 0.16, 0.4, 0.6, and 1.0, 1.4 and 2 g) were

applied to the hind paw plantar surfaces of mice with enough pressure to bend the filament. The absence of a paw being lifted after 5 s led to the use of the next filament with an increased force, whereas a lifted paw indicated a positive response, leading to the use of a subsequently weaker filament. Six measurements were collected for each mouse or until four consecutive positive or negative responses occurred. The 50% mechanical withdrawal threshold (expressed in g) was then calculated.

Spontaneous abdominal pain. Spontaneous abdominal pain was evaluated as previously reported⁶². Briefly, female mice were placed in a plexiglass cylinder and bottom-up video was recorded for 10 minutes. Abdominal licking was assessed by counting the number of times the mice groomed the abdominal region without moving to any other body area before or after the behavior. All videos were analyzed by blinded investigators.

Rotarod test. The locomotor function, balance, and sedation of mice were assessed after drug administration. Animals were trained on a rotarod apparatus (Ugo Basile) 24 h before the test. The day of the experiment, each mouse was individually placed on the apparatus, which accelerated from 4 to 40 rpm over the trial time of 300 s. Latency to fall was evaluated and recorded for three trials.

Plasmid construction

All short hairpin RNAs were designed according to Vector builder and RNAi Consortium of Broad Institute libraries. pAAV[FLEXon]-CMV > EGFP:LL:rev(mCherry:miR30-mC5ar1[shRNA#1]):rev(LL):WPRE and pAAV[FLEXon]-CMV > LL:rev(EGFP:5' miR-30E:{shRNA-NLRP1a};3' miR-30E):EGFP:5' miR-30E:{shRNA-NLRP1b};3' miR-30E:rev(LL):WPRE were used. pAAV[FLEXon]-CMV > EGFP-LL:rev(mCherry)-mNLRP3[miR30-shRNA]-rev(LL)-WPRE was generated in two steps. In the first step two overlapping fragments, were obtained by amplifying regions from pAAV[FLEXon]-CMV > EGFP-LL:rev(mCherry)-mC5ar1 [miR30-shRNA]-rev(LL)-WPRE with P1/P4 and P2/P3 primer couples. P1 and P2 were designed to include partial shNlrp3 overlapping regions. A third PCR, using external primers P3/P4 generated the extended fragment, that was cloned (AgeI/SpeI) into pAAV[Exp]-CMV > EGFP-LL:rev(mCherry)-mC5ar1 [miR30-shRNA]-rev(LL)-WPRE.

To obtain pAAV[Exp]-CMV > EGFP-LL:rev(mCherry)-mIL-1 β [miR30-shRNA]-rev(LL)-WPRE two oligonucleotides (P5 and P6) containing half short hairpin sequence were used to amplify a fragment from the pAAV[Exp]-CMV > EGFP:LL:rev(mCherry:miR30-mC5ar1[shRNA#1]):rev(LL):WPRE.

Purified product was phosphorylated with T4 PNK (NEB, #M0201S) according to the manufacturer instructions and finally subjected to circular ligation with a T4 ligase (Thermo Fisher #K1423). All the new-generated plasmids were validated by Sanger sequencing. Primer sequences are reported in Supplementary table S1.

AAV Generation

Recombinant AAV particles (rAAVs) were produced by using polyethylenimine (#23966, PEI, Polyscience) triple transfection strategy as previously described⁴⁶. In brief, AAVpro 293 T cells (#632273, Takara, RRID:CVCL_BOXW), were transfected with a 1:3 ratio of DNA:PEI⁶⁹. To obtain rAAVs, AAVpro 293 T cells were transiently transfected with 2.5 mg total DNA (plasmid expressing genes of interest, pAdDeltaF6; (#112867, Addgene) and Rep/Cap, 1:1:1 molar ratio). To infect with high-efficiency Schwann cells and primary sensor neurons, Rep/Cap 2/rh10 or 2/9n were used (pAAV2/rh10 #112866 or pAAV 2/9n #112865, respectively Addgene). rAAVs virions were extracted 72 h post-transfection, purified by iodixanol gradient ultracentrifugation, concentrated, and titrated using a RT-qPCR assay (#6233 AAVpro Titration Kit, Takara) according to the manufacturer instructions.

AAV production and cell lysis

AAVPro-HEK293T cells were cultured in DMEM supplemented with heat-inactivated FBS (10%), Pen/Strep (1%), and L-glutamine (2%) and sodium pyruvate (1%). Three days before transfection, cells were seeded in a CellBIND Polystyrene CellSTACK 2 Chamber (#3310, Corning, Corning, NY, USA) for 48 h to reach 80% confluence. Cells were washed with PBS, detached with trypsin-EDTA 0.05% (EuroClone, Milan, Italy). Finally, 250 million cells were seeded in a CellBIND Polystyrene CellSTACK 5 Chamber (#3311; Corning) for 24 h, until 80% of confluence. Each chamber was transfected with 2.5 mg of DNA containing the three plasmids (packaging, helper and GOI plasmids) in a 1:1:1 molar ratio. Total DNA was diluted in 176 ml of OptiMEM (Thermo Fisher Scientific) and combined with PEI (1:3 DNA to PEI ratio). After 15 min of incubation, 350 mL of DMEM supplemented with FBS (2%) was added to the OptiMEM/DNA/PEI mix and used to replace the complete medium in each chamber. Cells were left at 37 °C for 72 h, before AAV particles were started to be collected. Cells were harvested and transferred into 50 mL conical tubes and centrifuged at 1000 × g for 10 min at 4 °C. The supernatant was filtered through 0.45- μ m PES membranes, before that 25 mL of PEG solution (400 g of 40% polyethylene glycol + 24 g of NaCl in ddH₂O to a final volume of 1.000 mL) was added to every 100 mL of supernatant. The total solution was slowly stirred at 4 °C for 1 h and then, kept for 3 h without stirring at 4 °C to allow full precipitation of particles. The solution was then centrifuged at 2.800 × g for 15 min at 4 °C, the supernatant was discarded, and the virus was resuspended in a 10 mL of PBS/pluronic F68 (0.001%)/NaCl (200 mM) solution. Virus-producing cell pellet was directly resuspended in 10 mL of PBS/Pluronic F68 (0.001%)/NaCl (200 mM) solution and cells were lysed by 4 cycles of freezing/thaw. Each cycle included a step of 30 min at -80 °C, followed by a quick thaw at 37 °C for 10 min. Sample was then centrifuged at 3.200 × g for 15 min at 4 °C and supernatant, containing the AAV particles was collected, while cell debris were discarded. Samples obtained by medium treatment and cell lyses, containing the AAV particles, were finally mixed, incubated with benzonase (50 U/mL) at 37 °C for 45 min to digest residual plasmids and residual genomic DNA / cellular RNA. Then, sample was centrifuged at 2.400 × g for 10 min at 4 °C. The clarified supernatant was transferred to new tubes and was kept overnight at 4 °C before purification.

Iodixanol-based purification protocol

Purification using a gradient of iodixanol was prepared as previously described¹ with a few modifications. Starting with a 60% iodixanol solution (OptiPrep; STEMCELL Technologies, Vancouver, Canada), a gradient was prepared with a 15% solution [4.5 mL of iodixanol (60%) + 13.5 mL of NaCl/PBS-MK buffer (1 M)], a 25% solution [5 mL of iodixanol (60%) + 7 mL of PBS-MK buffer (1×) + 30 μ L of phenol red], a 40% solution [6.7 mL of iodixanol (60%) + 3.3 mL of PBS-MK buffer (1×)], and a 60% solution [10 mL of iodixanol (60%) + 45 μ L of phenol red]. Each solution was added into a 39-mL Quick-Seal tube (Beckman Coulter, Brea, CA, USA) using a syringe equipped with an 18 G needle in the following order: 8 mL of the iodixanol solution (15%), 6 mL of the iodixanol solution (25%), 5 mL of the iodixanol solution (40%), and 5 mL of the iodixanol solution (60%). Finally, tubes were filled with the sample, sealed and, centrifuged in a Type 70 Ti rotor (Beckman Coulter) at 350.000 × g at 10 °C for 90 min and then pierced with a 16 G needle on top and an 18 G needle at the interface between the 60% and 40% iodixanol gradients. Viral particles contained in the 40% iodixanol layer were fractionated in 1.5 mL microcentrifuge tubes and concentrated using Amicon Ultra-15 centrifugal filter units (molecular weight cut-off, 100 kDa; Merck Millipore). Before the concentration step, membranes were covered with 15 mL of 0.1% Pluronic F68 in PBS solution that were discarded and replaced with 15 mL of 0.01% Pluronic F68 in PBS solution. The tubes were centrifuged at 3.000 rpm for 5 min at 4 °C. The supernatant was discarded, and 15 mL of 0.001% Pluronic

F68 in PBS + NaCl 200 mM solution was added and centrifuged at 3,000 rpm for 5 min at 4 °C. The sample was then added and centrifuged at 3,500 rpm for 8 min at 4 °C and flowthrough was discarded. During concentration process, formulation buffer (0.001% Pluronic F68 in PBS) was also added to the sample after few centrifugation steps to replace iodixanol and to avoid toxicity in animals after AAV injection. The viral titer was quantified using RT-qPCR.

Immunofluorescence

Mice were anesthetized, transcardially perfused with PBS (phosphate buffer saline), and then tissues (trigeminal, sciatic nerve and endometrial lesions) were collected. The collected tissues from perfused mice were placed overnight at 4 °C in 10% formalin, transferred to 30% sucrose overnight, frozen, and cryosectioned at 10 μm. Endometrial lesions were stained with hematoxylin and eosin (H&E) for histological examination. After blocking using normal donkey serum (NDS, 5%) for 1 h sciatic and trigeminal nerve tissue were incubated with the following primary antibodies: F4/80 (#MA516624, rat monoclonal (Cl:A3-1), Thermo Fisher Scientific, 1:50, RRID:AB_253820), C5aR1 (#orb393229, rabbit polyclonal, Biorbyt Ltd, 1:100), C5aR1 (#MCA2456GA, rat monoclonal, Bio-Rad, 1:100, RRID:AB_770091), NLRP3 (#MA5-32255, rabbit monoclonal, Thermo Fisher Scientific, 1:100, RRID:AB_2809541), NLRP1 (#12256-1-AP, rabbit polyclonal, Proteintech, 1:50, RRID:AB_2298504) and IL-1β (#NB600-633, rabbit polyclonal, Novus Biological, 1:100, RRID:AB_10001060) for 1 h at room temperature and O/N at 4 °C with SOX10 (#AF2864, goat polyclonal, R&D Systems, 1:200, RRID:AB_442208). Sections were then incubated for 2 h in the dark with the following with fluorescent secondary antibodies: Alexa Fluor 488 (#A32790, donkey anti-rabbit polyclonal, Thermo Fisher Scientific, 1:600, RRID:AB_2762833), Alexa Fluor 488 (#A21208, donkey anti-rat polyclonal, Thermo Fisher Scientific, 1:600, RRID:AB_2535794) and Alexa Fluor 594 (#A11058, donkey anti-goat polyclonal, Thermo Fisher Scientific, 1:600, RRID:AB_2534105). Sections were coverslipped using a water-based mounting medium containing DAPI (#ab104139; Abcam). Specificity of C5aR1, NLRP3 and NLRP1 antibody was tested in HEK293T cells and HEK293T cells overexpressing the murine C5aR1 NLRP3 and NLRP1a and NLRP1b respectively (HEK293T-C5aR1, Nlrp3 and Nlrp1a and Nlrp1a (Supplementary Fig. 7). Briefly, cells were washed in PBS and fixed in 10% formalin at 4 °C for 15 min, followed by permeabilization with 0.3% Triton X-100 for 10 min RT. Blocking was performed using a mixture of normal goat serum (NGS, 5%) and bovine serum albumin (BSA, 5%) for 1 h. Cells were then washed twice in PBS and incubated with the primary antibodies C5aR1 (#orb393229, rabbit polyclonal, Biorbyt Ltd, 1:100), NLRP1 (#12256-1-AP, rabbit polyclonal, Proteintech, 1:200, RRID:AB_2298504) and NLRP3 (#MA5-32255, rabbit monoclonal, Thermo Fisher Scientific, 1:100, RRID:AB_2809541) for 1 h RT, following by a fluorescent polyclonal secondary antibody Alexa Fluor 488 (#A32731, goat anti-rabbit polyclonal, Thermo Fisher Scientific, 1:600, RRID:AB_2633280) for 2 h RT in the dark. Cells were then washed twice and mounted using a water-based mounting medium with 4',6'-diamidino-2-phenylindole (DAPI, #ab104139; Abcam). All slides were visualized and analyzed using a Zeiss Axio Imager 2 microscope with Z-stacks in the Aptome mode (ZEISS). The number of F4/80⁺ cells was counted in 4.5 × 10⁵ μm² boxes in the sciatic nerve and trigeminal nerve trunk. Pearson correlation (Rcoloc) value in the colocalization analysis were calculated using the colocalization Plugin of the ImageJ (v.1.54 f; National Institutes of Health, Bethesda, MD, USA).

Frozen sections of mouse trigeminal and sciatic nerve were incubated with an anti-4-HNE (#ab48506, mouse monoclonal (HNEJ-2), Abcam, 1:25, RRID:AB_867452), diluted in the blocking solution (NGS, 5%) for 1 h at room temperature. Sections were then incubated for 2 h in the dark with fluorescent secondary antibody polyclonal Alexa Fluor 647 (#A-21236, goat anti-mouse polyclonal, Thermo Fisher Scientific, 1:600, RRID:AB_2535805), then washed and coverslipped using a water-based mounting medium with DAPI (#ab104139, Abcam).

The 4-HNE staining was evaluated as the fluorescence intensity measured by an image processing program (ImageJ 1.32J, National Institutes of Health).

RNAScope

Frozen tissue sections (10 μm) of mouse sciatic nerve were washed with 1× PBS, baked for 30 min at 60 °C, post-fixed with 4% paraformaldehyde in 1× PBS at 4 °C, and dehydrated. Sciatic nerve tissues were treated with hydrogen peroxide (#322335; Advanced Cell Diagnostics, Newark, CA, USA) for 10 min at RT. Target retrieval was performed for 5 min at 99–100 °C, followed by Protease III (#322337; Advanced Cell Diagnostics) pre-treatment for 30 min at 40 °C. Samples were subsequently hybridized with a probes specific to mouse *Nlrp1a* (#499091; Advanced Cell Diagnostics), *Nlrp1b* (#1076671-C1; Advanced Cell Diagnostics), *Nlrp3* (#439571; Advanced Cell Diagnostics), *C5aR1* (#439951; Advanced Cell Diagnostics) for 2 h at 40 °C. Sequential signal amplification and green chromogenic detection was performed. Sciatic nerve slides were subjected to immunofluorescence labeling using Alexa Fluor® 647 anti-S100 beta antibody [EP1576Y] (#ab196175; anti-rabbit monoclonal, Abcam, 1:50, RRID:AB_2868562). Sciatic nerve sections were coverslipped and mounted using a water-based mounting medium with DAPI (#ab104139; Abcam). Fluorescent images were acquired using a Zeiss Axio Imager 2 (ZEISS).

Proteome profiler array

Mouse plasma samples were collected at different days after endometriosis induction for a cytokine array analysis using the Proteome Profiler Mouse Cytokine Array Kit, Panel A (#ARY006, R&D Systems) according to manufacturer's instructions. Signal was developed using an imaging system (ChemiDoc; Bio-Rad). The density of specific cytokine dots was measured using HLIimage⁺⁺ (v. PCM.25.5.1.a).

Caspase-Glo® 1 Inflammasome Assay

The caspase-1 activity was evaluated using the bioluminescent-based assay Caspase-Glo® 1 inflammasome assay (#TM456, Promega) according to manufacturer's instructions. Briefly, HSCs were grown on in 96-well poly-L-lysine-coated (8.3 μM) plates and incubated with C5a (100 ng/ml) in the presence of DF2593A (1 μM), Ac-YVAD-CHO (1 μM) or veh (0.001% DMSO) at 37 °C in 5% CO₂ and 95% O₂. After 16 h, the cell culture medium was collected and transferred to a 96-white, opaque-walled-multiwell plates (with a clear bottom) (#6005181, PerkinElmer) and incubated with Caspase-Glo® 1 Reagent for 60 min. The luminescence signal was measured by FlexStation3 Multi-Mode Microplate Reader (Molecular Devices;) using SoftMax® Pro7 software (Molecular Devices). Results were expressed as relative light units (RLU).

Caspase-1 in vitro imaging

The genetically encoded fluorescent sensor Single-Cell Imaging of Caspase-1 (SCAT1) based on fluorescence resonance energy transfer (FRET) was used to detect the inflammasome-mediated caspase-1 activation in HSCs. Briefly, HSCs were plated on 96-well poly-L-lysine-coated (8.3 μM) black clear bottom (5 × 10⁵ cells/well; #6055302 PerkinElmer) and transfected with cDNA of SCAT1 (130-300 ng) using jetOPTIMUS® DNA transfection reagent (#55-250, Polyplus) for 16-24 h at 37 °C in 5% CO₂ and 95% O₂. On the day of experiments, HSCs were washed and added with HBSS at pH 7.4 at 37 °C and transferred to a chamber on the stage of a fluorescent microscope for recording (Axio Observer 7; with a fast filter wheel and Digi-4 lens to record excitations and Ultra-fast Sutter Lambda DG4 Xenon excitation source-range 300-700 nm) (Zeiss) with 20x objective. Cells were exposed to C5a (10 μg/ml) in the presence of DF2593A (1 μM) or Ac-YVAD-CHO (1 μM) vehicle (0.001% DMSO). FRET changes were measured as a ratio of the acceptor fluorophore emission (530 nm) to donor emission (435 nm). The ΔF/F0 ratio was calculated for each experiment and the results were expressed as the AUC after inverting the curve.

C5a and IL-1 β assays

C5a and IL-1 β content was assayed in mouse sciatic and trigeminal nerve tissue homogenates and in mouse plasma samples using a single-analyte enzyme-linked immunosorbent assay (ELISA) kit (#ab193718 and #ab197742, Abcam, Cambridge, UK) according to the manufacturer's protocol. Data are expressed as pg/mg of protein and pg/mL. C5a and IL-1 β content was assayed in human plasma samples and HSCs cultured medium by ELISA kit (#ab193695 and #ab214025, Abcam) according to the manufacturer's protocol. Data are expressed as pg/mL.

Reverse transcription-quantitative real-time PCR (RT-qPCR)

Total RNA was extracted from HSCs, primary MSCs, and liver tissue homogenates using the RNeasy Mini Kit (Qiagen SpA, Hilden, Germany), according to the manufacturer's protocol. RNA concentration and purity were assessed spectrophotometrically by measuring the absorbance at 260 and 280 nm. RNA was reverse transcribed using the Qiagen QuantiTect Reverse Transcription Kit (Qiagen SpA, Hilden, Germany) following the manufacturer's protocol. For relative mRNA quantification, RT-PCR was performed using Rotor Gene[®] Q software (v.2.3.1.49; Qiagen SpA). The relative abundance of mRNA transcripts was calculated using the Δ^{CT} method and normalized to glyceraldehyde-3-phosphate dehydrogenase (GAPDH) levels. The sets of primers are reported in Supplementary Table S2.

Trans-well migration assay

Noncontact coculture transwell cell culture system between macrophages and Schwann cells was obtained using the Boyden migration assay⁶¹. Briefly, the noncontact cocultured cells were prepared as follows: macrophage-like U937 cells or RAW 264.7 were seeded at a density of 2.5×10^4 / chamber into the upper of a 24-well transwell cell culture system (6.5 mm in diameter, with 8- μm pores, (#CLS3458™; Corning) by using the complete media described above and allowed to grow 2 days after PMA treatment (U937 cells) or overnight (RAW 264.7) before migration assay⁷⁰. In the meantime, HSCs and MSCs were plated on a 24-well plate. On the day of the experiment, all the cells were replaced with serum-free media, and the macrophage-like U937 cells and RAW 264.7 cells cultured on the membrane of 24-well transwell insert were placed into the 24-well plate cultures containing the HSCs and MSCs to initiate the experiment. HSCs and MSCs were treated with C5a (100 ng/ml) also in the presence of DF2593A (1 μM) or veh (0.001% DMSO) or in the presence mAb-IL-1 β (1 $\mu\text{g}/\text{ml}$) or IgG control (1 $\mu\text{g}/\text{ml}$). After 16 h of incubation, migrated cells on the lower surface of the filter were fixed and stained with Diffquick staining set following the manufacturer's directions (#726443™), and nonmigratory cells on the upper surface of the filter were wiped with a cotton swab. Random fields were counted under a light microscope using a 20x objective ($1.5 \times 10^5 \mu\text{m}^2$).

Statistical analysis

Data are presented as mean \pm SEM. For multiple comparisons, a one-way ANOVA followed by a post-hoc Bonferroni's test was used. The two groups were compared using Student's t-test. For behavioral experiments with repeated measures, a two-way mixed-model ANOVA followed by a post hoc Bonferroni's test was used. Statistical analyses were performed on raw data using GraphPad Prism 8 (GraphPad Software Inc.). *P* values less than 0.05 ($P < 0.05$) were considered significant. EC50 values were determined from non-linear regression models using GraphPad Prism 8. The statistical tests used and sample size for each analysis are shown in the Fig. legends.

Reporting summary

Further information on research design is available in the Nature Portfolio Reporting Summary linked to this article.

Data availability

Materials are available upon request from Francesco De Logu (francesco.delogu@unifi.it) or Romina Nassini (romina.nassinini@unifi.it). All data supporting the findings described in this manuscript is also available upon request from Francesco De Logu (francesco.delogu@unifi.it) or Romina Nassini (romina.nassinini@unifi.it). All data generated from this study are provided in the Supplementary Information/Source Data file. Source data are provided with this paper.

References

- International Working Group of Aagl EE. et al. An international terminology for endometriosis, (2021). *Hum. Reprod. Open* **2021**, hoab029 (2021).
- Giudice, L. C. & Kao, L. C. Endometriosis. *Lancet* **364**, 1789–1799 (2004).
- Parasar, P., Ozcan, P. & Terry, K. L. Endometriosis: Epidemiology, Diagnosis and Clinical Management. *Curr. Obstet. Gynecol. Rep.* **6**, 34–41 (2017).
- Mao, A. J. & Anastasi, J. K. Diagnosis and management of endometriosis: the role of the advanced practice nurse in primary care. *J. Am. Acad. Nurse Pr.* **22**, 109–116 (2010).
- Jenabi, E. & Khazaei, S. Endometriosis and migraine headache risk: a meta-analysis. *Women Health* **60**, 939–945 (2020).
- Nagai, K. et al. Disease history and risk of comorbidity in women's life course: a comprehensive analysis of the Japan Nurses' Health Study baseline survey. *BMJ Open* **5**, e006360 (2015).
- Yang, M. H. et al. Women with endometriosis are more likely to suffer from migraines: a population-based study. *PLoS One* **7**, e33941 (2012).
- Ferrero, S. et al. Increased frequency of migraine among women with endometriosis. *Hum. Reprod.* **19**, 2927–2932 (2004).
- Larrosa Pardo, F., Bondesson, E., Schelin, M. E. C. & Jöud, A. A diagnosis of rheumatoid arthritis, endometriosis or IBD is associated with later onset of fibromyalgia and chronic widespread pain. *Eur. J. Pain.* **23**, 1563–1573 (2019).
- Greenbaum, H., Weil, C., Chodick, G., Shalev, V. & Eisenberg, V. H. Evidence for an association between endometriosis, fibromyalgia, and autoimmune diseases. *Am. J. Reprod. Immunol.* **81**, e13095 (2019).
- Walport, M. J. Complement. First of two parts. *N. Engl. J. Med* **344**, 1058–1066 (2001).
- West, E. E. & Kemper, C. Complosome - the intracellular complement system. *Nat. Rev. Nephrol.* **19**, 426–439 (2023).
- Ricklin, D., Hajishengallis, G., Yang, K. & Lambris, J. D. Complement: a key system for immune surveillance and homeostasis. *Nat. Immunol.* **11**, 785–797 (2010).
- Dunkelberger, J. R. & Song, W. C. Complement and its role in innate and adaptive immune responses. *Cell Res* **20**, 34–50 (2010).
- Monk, P. N., Scola, A. M., Madala, P. & Fairlie, D. P. Function, structure and therapeutic potential of complement C5a receptors. *Br. J. Pharm.* **152**, 429–448 (2007).
- Clark, J. D. et al. Blockade of the complement C5a receptor reduces incisional allodynia, edema, and cytokine expression. *Anesthesiology* **104**, 1274–1282 (2006).
- Liang, D. Y. et al. The complement component C5a receptor mediates pain and inflammation in a postsurgical pain model. *Pain* **153**, 366–372 (2012).
- Ting, E. et al. Role of complement C5a in mechanical inflammatory hypernociception: potential use of C5a receptor antagonists to control inflammatory pain. *Br. J. Pharm.* **153**, 1043–1053 (2008).
- Moriconi, A. et al. Targeting the minor pocket of C5aR for the rational design of an oral allosteric inhibitor for inflammatory and neuropathic pain relief. *Proc. Natl Acad. Sci. USA* **111**, 16937–16942 (2014).

20. Revised American Society for Reproductive Medicine classification of endometriosis: 1996. *Fertil. Steril.* **67**, 817–821 (1997).
21. Karadadas, E. et al. Evaluation of complement system proteins C3a, C5a and C6 in patients of endometriosis. *Clin. Biochem* **81**, 15–19 (2020).
22. Ahn, S. H. et al. Pathophysiology and Immune Dysfunction in Endometriosis. *Biomed. Res Int* **2015**, 795976 (2015).
23. Takebayashi, A. et al. Subpopulations of macrophages within eutopic endometrium of endometriosis patients. *Am. J. Reprod. Immunol.* **73**, 221–231 (2015).
24. Scheerer, C. et al. Characterization of endometriosis-associated immune cell infiltrates (EMaICI). *Arch. Gynecol. Obstet.* **294**, 657–664 (2016).
25. Quadros A. U. et al. Complement receptor C5aR1 signaling in sensory neuron-associated macrophages drives neuropathic pain. *bioRxiv*, 2022.2007.2001.498487 (2022).
26. De Logu, F. et al. Schwann cell TRPA1 mediates neuroinflammation that sustains macrophage-dependent neuropathic pain in mice. *Nat. Commun.* **8**, 1887 (2017).
27. De Logu, F. et al. Peripheral Nerve Resident Macrophages and Schwann Cells Mediate Cancer-Induced Pain. *Cancer Res* **81**, 3387–3401 (2021).
28. De Logu, F. et al. Macrophages and Schwann cell TRPA1 mediate chronic allodynia in a mouse model of complex regional pain syndrome type I. *Brain Behav. Immun.* **88**, 535–546 (2020).
29. Landini L. et al. TRPA1 Role in Inflammatory Disorders: What Is Known So Far? *Int. J. Mol. Sci.* **23**, (2022).
30. Ahn, S. H. et al. Immune-inflammation gene signatures in endometriosis patients. *Fertil. Steril.* **106**, 1420–1431.e1427 (2016).
31. Morgan, B. P., Boyd, C. & Bubeck, D. Molecular cell biology of complement membrane attack. *Semin Cell Dev. Biol.* **72**, 124–132 (2017).
32. Fluiter, K., Opperhuizen, A. L., Morgan, B. P., Baas, F. & Ramaglia, V. Inhibition of the membrane attack complex of the complement system reduces secondary neuroaxonal loss and promotes neurologic recovery after traumatic brain injury in mice. *J. Immunol.* **192**, 2339–2348 (2014).
33. Greaves, E. et al. Estradiol is a critical mediator of macrophage-nerve cross talk in peritoneal endometriosis. *Am. J. Pathol.* **185**, 2286–2297 (2015).
34. Wu, J., Xie, H., Yao, S. & Liang, Y. Macrophage and nerve interaction in endometriosis. *J. Neuroinflamm.* **14**, 53 (2017).
35. Burnett, S. H. et al. Conditional macrophage ablation in transgenic mice expressing a Fas-based suicide gene. *J. Leukoc. Biol.* **75**, 612–623 (2004).
36. Shepherd, A. J. et al. Macrophage angiotensin II type 2 receptor triggers neuropathic pain. *Proc. Natl Acad. Sci. USA* **115**, E8057–E8066 (2018).
37. Yim, A. K. Y. et al. Disentangling glial diversity in peripheral nerves at single-nuclei resolution. *Nat. Neurosci.* **25**, 238–251 (2022).
38. Carvalho, K. et al. Modulation of C5a-C5aR1 signaling alters the dynamics of AD progression. *J. Neuroinflamm.* **19**, 178 (2022).
39. Wang, H. A., Lee, J. D., Lee, K. M., Woodruff, T. M. & Noakes, P. G. Complement C5a-C5aR1 signalling drives skeletal muscle macrophage recruitment in the hSOD1(G93A) mouse model of amyotrophic lateral sclerosis. *Skelet. Muscle* **7**, 10 (2017).
40. Luan, X. et al. Blockade of C5a receptor unleashes tumor-associated macrophage antitumor response and enhances CXCL9-dependent CD8(+) T cell activity. *Mol. Ther.* **32**, 469–489 (2024).
41. Jang, J. H. et al. Nociceptive sensitization by complement C5a and C3a in mouse. *Pain* **148**, 343–352 (2010).
42. Arbore, G. & Kemper, C. A novel “complement-metabolism-inflammation axis” as a key regulator of immune cell effector function. *Eur. J. Immunol.* **46**, 1563–1573 (2016).
43. Liu, T. et al. Single-cell imaging of caspase-1 dynamics reveals an all-or-none inflammasome signaling response. *Cell Rep.* **8**, 974–982 (2014).
44. Vanaja, S. K., Rathinam, V. A. & Fitzgerald, K. A. Mechanisms of inflammasome activation: recent advances and novel insights. *Trends Cell Biol.* **25**, 308–315 (2015).
45. Rider, P. et al. IL-1 α and IL-1 β recruit different myeloid cells and promote different stages of sterile inflammation. *J. Immunol.* **187**, 4835–4843 (2011).
46. Landini, L. et al. Schwann cell insulin-like growth factor receptor type-1 mediates metastatic bone cancer pain in mice. *Brain Behav. Immun.* **110**, 348–364 (2023).
47. Aslan, C. et al. Overexpression of complement C5 in endometriosis. *Clin. Biochem* **47**, 496–498 (2014).
48. Capobianco, A. Rovere-Querini P. Endometriosis, a disease of the macrophage. *Front Immunol.* **4**, 9 (2013).
49. Haggadone, M. D., Grailer, J. J., Fattahi, F., Zetoune, F. S. & Ward, P. A. Bidirectional Crosstalk between C5a Receptors and the NLRP3 Inflammasome in Macrophages and Monocytes. *Mediat. Inflamm.* **2016**, 1340156 (2016).
50. Yu, S. et al. The complement receptor C5aR2 promotes protein kinase R expression and contributes to NLRP3 inflammasome activation and HMGB1 release from macrophages. *J. Biol. Chem.* **294**, 8384–8394 (2019).
51. Arbore, G. et al. T helper 1 immunity requires complement-driven NLRP3 inflammasome activity in CD4(+) T cells. *Science* **352**, aad1210 (2016).
52. Grace, P. M. et al. Morphine paradoxically prolongs neuropathic pain in rats by amplifying spinal NLRP3 inflammasome activation. *Proc. Natl Acad. Sci. USA* **113**, E3441–E3450 (2016).
53. Khan, N., Kuo, A., Brockman, D. A., Cooper, M. A. & Smith, M. T. Pharmacological inhibition of the NLRP3 inflammasome as a potential target for multiple sclerosis induced central neuropathic pain. *Inflammopharmacology* **26**, 77–86 (2018).
54. Chen, R., Yin, C., Fang, J. & Liu, B. The NLRP3 inflammasome: an emerging therapeutic target for chronic pain. *J. Neuroinflamm.* **18**, 84 (2021).
55. Han, S. J. et al. Estrogen Receptor beta Modulates Apoptosis Complexes and the Inflammasome to Drive the Pathogenesis of Endometriosis. *Cell* **163**, 960–974 (2015).
56. Murakami, M. et al. Effectiveness of NLRP3 Inhibitor as a Non-Hormonal Treatment for ovarian endometriosis. *Reprod. Biol. Endocrinol.* **20**, 58 (2022).
57. Guo, X. et al. NLRP3 Inflammasome Activation of Mast Cells by Estrogen via the Nuclear-Initiated Signaling Pathway Contributes to the Development of Endometriosis. *Front Immunol.* **12**, 749979 (2021).
58. Tietjen, G. E. et al. Endometriosis is associated with prevalence of comorbid conditions in migraine. *Headache* **47**, 1069–1078 (2007).
59. Faul, F., Erdfelder, E., Buchner, A. & Lang, A. G. Statistical power analyses using G*Power 3.1: tests for correlation and regression analyses. *Behav. Res Methods* **41**, 1149–1160 (2009).
60. De Logu, F. et al. Schwann cell endosome CGRP signals elicit periorbital mechanical allodynia in mice. *Nat. Commun.* **13**, 646 (2022).
61. Yang, C. Y. et al. Triptolide represses oral cancer cell proliferation, invasion, migration, and angiogenesis in co-inoculation with U937 cells. *Clin. Oral. Investig.* **21**, 419–427 (2017).
62. Fattori, V. et al. Nonsurgical mouse model of endometriosis-associated pain that responds to clinically active drugs. *Pain* **161**, 1321–1331 (2020).
63. Jain, P. et al. Behavioral and molecular processing of visceral pain in the brain of mice: impact of colitis and psychological stress. *Front Behav. Neurosci.* **9**, 177 (2015).

64. Chaplan, S. R., Bach, F. W., Pogrel, J. W., Chung, J. M. & Yaksh, T. L. Quantitative assessment of tactile allodynia in the rat paw. *J. Neurosci. Methods* **53**, 55–63 (1994).
65. Elliott, M. B., Oshinsky, M. L., Amenta, P. S., Awe, O. O. & Jallo, J. I. Nociceptive neuropeptide increases and periorbital allodynia in a model of traumatic brain injury. *Headache* **52**, 966–984 (2012).
66. Marone, I. M. et al. TRPA1/NOX in the soma of trigeminal ganglion neurons mediates migraine-related pain of glyceryl trinitrate in mice. *Brain* **141**, 2312–2328 (2018).
67. De Logu, F. et al. Migraine-provoking substances evoke periorbital allodynia in mice. *J. Headache Pain*. **20**, 18 (2019).
68. Dixon, W. J. Efficient analysis of experimental observations. *Annu Rev. Pharm. Toxicol.* **20**, 441–462 (1980).
69. Durocher, Y., Perret, S. & Kamen, A. High-level and high-throughput recombinant protein production by transient transfection of suspension-growing human 293-EBNA1 cells. *Nucleic Acids Res.* **30**, E9 (2002).
70. Guy J. B. et al. Evaluation of the Cell Invasion and Migration Process: A Comparison of the Video Microscope-based Scratch Wound Assay and the Boyden Chamber Assay. *J. Vis. Exp.* (2017).

designed and conducted the experiments, performed the analysis, discussed the results. R.N., F.D.L. supervised the study and wrote the manuscript.

Competing interests

R.N., F.D.L. and P.G. are founding scientists of FloNext Srl. G.B. is fully employed at FloNext Srl, Italy. Other authors declare no competing interests.

Additional information

Supplementary information The online version contains supplementary material available at <https://doi.org/10.1038/s41467-024-54486-6>.

Correspondence and requests for materials should be addressed to Romina Nassini or Francesco De Logu.

Peer review information *Nature Communications* thanks Gang Chen, Usachev Yuriy and the other anonymous reviewer(s) for their contribution to the peer review of this work. A peer review file is available.

Reprints and permissions information is available at <http://www.nature.com/reprints>

Publisher's note Springer Nature remains neutral with regard to jurisdictional claims in published maps and institutional affiliations.

Open Access This article is licensed under a Creative Commons Attribution-NonCommercial-NoDerivatives 4.0 International License, which permits any non-commercial use, sharing, distribution and reproduction in any medium or format, as long as you give appropriate credit to the original author(s) and the source, provide a link to the Creative Commons licence, and indicate if you modified the licensed material. You do not have permission under this licence to share adapted material derived from this article or parts of it. The images or other third party material in this article are included in the article's Creative Commons licence, unless indicated otherwise in a credit line to the material. If material is not included in the article's Creative Commons licence and your intended use is not permitted by statutory regulation or exceeds the permitted use, you will need to obtain permission directly from the copyright holder. To view a copy of this licence, visit <http://creativecommons.org/licenses/by-nc-nd/4.0/>.

© The Author(s) 2024

Acknowledgements

Supported by grants from: Fondazione Telethon (Grant no GMR22T1070) (F.D.L.), IBSA Foundation Fellowship 2023 (F.D.L.), European Research Council (ERC) under the European Union's Horizon 2020 research and innovation programme (grant agreement No. 835286) (P.G.), Ministero della Salute GR-2018-12368352 (Bando Salute 2018) (V.S.), European Union - Next Generation EU - Funding for the promotion and development of the policies of the National Program for search (PNR) DM737/2021 MUR - Call UNIFI Problem-driven - Project tArgetiNg Schwann cells for chronic gEndeR pain - Answer - CUP B55F21007810001 (R.N.), European Union - Next Generation EU, National Recovery and Resilience Plan, Mission 4 Component 2 - Investment 1.4 - National Center for Gene Therapy and Drugs based on RNA Technology - CUP B13C22001010001 (R.N.) and NEXTGENERATIONEU (NGEU) funded by the Ministry of University and Research (MUR), National Recovery and Resilience Plan (NRRP), project MNESYS (PE0000006) – A Multiscale integrated approach to the study of the nervous system in health and disease (DR. 1553 11.10.2022) (P.G., F.D.L.). Views and opinions expressed are however those of the author(s) only and do not necessarily reflect those of the European Union or the European Commission.

Author contributions

M.T., L.L., D.S.M.de A., M.M., V.S., M.C., P.P., M.Mo., G.D.S., B.P., S.V., L.F.I., T.M.C., G.B., E.B., I.S., A.M., M.T., M.Di T., F.P., P.G., R.N., F.D.L.